RESEARCH ARTICLE | APRIL 15 2026

Achromatic interfacial Cherenkov radiation from photonic crystals

Xiangfeng Xi ; Zheng Gong ; Ruoxi Chen ; Zun Wang; Owen D. Miller ; Yi Yang ; Hongsheng Chen ; Ido Kaminer ; Xiao Lin

Appl. Phys. Rev. 13, 021407 (2026)
https://doi.org/10.1063/5.0316387

Applied Physics Reviews ARTICLE pubs.aip.org/aip/are

Achromatic interfacial Cherenkov radiation from photonic crystals

Cite as: Appl. Phys. Rev. **13**, 021407 (2026); doi: 10.1063/5.0316387
Submitted: 12 December 2025 · Accepted: 31 March 2026 ·
Published Online: 15 April 2026

Xiangfeng Xi,[1] Zheng Gong,[1] Ruoxi Chen,[1] Zun Wang,[1] Owen D. Miller,[2] Yi Yang,[3] Hongsheng Chen,[1,a)] Ido Kaminer,[4,a)] and Xiao Lin[1,a)]

AFFILIATIONS

[1]State Key Laboratory of Extreme Photonics and Instrumentation, Zhejiang Key Laboratory of Intelligent Electromagnetic Control and Advanced Electronic Integration, College of Information Science & Electronic Engineering, Zhejiang University, Hangzhou 310027, China
[2]Department of Applied Physics and Energy Sciences Institute, Yale University, New Haven, Connecticut 06520, USA
[3]Department of Physics, University of Hong Kong, Hong Kong 999077, China
[4]Department of Electrical and Computer Engineering, Technion-Israel Institute of Technology, Haifa 32000, Israel

[a)]**Authors to whom correspondence should be addressed:** hansomchen@zju.edu.cn; kaminer@technion.ac.il; and xiaolinzju@zju.edu.cn

ABSTRACT

Interfacial Cherenkov radiation originates from the interaction of charged particles with sequential interfaces inside photonic crystals and is crucial to many applications, ranging from particle detectors and lasers to electron microscopy and spectroscopy, since it can create directional light emission at arbitrary spectra. However, the interfacial Cherenkov radiation suffers from chromatic issues and is featured with frequency-sensitive radiation angles due to the intrinsic structural dispersion of photonic crystals. Counterintuitively, here we reveal a universal mechanism to create the broadband achromatic interfacial Cherenkov radiation from photonic crystals. Our mechanism exploits the anomalous Maxwell-Garnett theory beyond the long-wavelength limit via the Brewster effect and introduces it for the first time into the context of Cherenkov radiation. Specifically, we present photonic crystal designs that mimic homogeneous achromatic media in terms of their interfacial Cherenkov radiation, emitted precisely at the Brewster angle. We find the radiation peak angle could be frequency-insensitive, even over the entire visible spectrum.

INTRODUCTION

Cherenkov radiation offers a compelling effect to create directional light emission at arbitrary spectral regimes.[1–3] This effect thus finds exotic uses in both basic science and practical applications in various realms, ranging from cosmology,[4,5] high-energy physics,[6–9] nanophotonics,[10–14] plasmonics,[15–17] and materials science,[18,19] to imaging,[20–23] photodynamic therapy[24,25] and vacuum electronics.[26,27] However, since the conventional Cherenkov radiation is a *bulk effect*, originating from the interaction of moving charged particles with bulk materials, its emergence requires particle velocities faster than the so-called Cherenkov threshold, namely, the phase velocity of light in the host bulk material. As a result, all these applications of bulk Cherenkov radiation are strictly limited by the particle velocity and the material property. As a typical example, the particle detector based on bulk Cherenkov radiation generally requires the usage of specific materials with their refractive index very close to unity, which are often restricted to silicon aerogels or large gas chambers, for the identification of high-energy particles in the giga-electron-volt (GeV) range.[28]

To tackle this issue, Refs. 7 and 29 recently revealed a brand-new way to create the effective Cherenkov radiation by exploiting the *interface effect*, namely, the interaction of moving charged particles with sequential interfaces inside photonic crystals, rather than the bulk effect. This way, the interfacial Cherenkov radiation from photonic crystals fundamentally overcomes the velocity and material limitations for conventional bulk Cherenkov radiation and holds great promise for the development of many enticing on-chip photonic devices.[30–33] One promising application of interfacial Cherenkov radiation is the design of integrated light sources[34–37] at previously hard-to-reach frequencies via low-velocity charged particles. This is because the interfacial Cherenkov radiation is intrinsically threshold-free and can be excited by ultralow-energy charged particles with their kinetic

energy down to several electron-volts (eV).[29] Another potential application of interfacial Cherenkov radiation is the development of miniaturized Cherenkov detectors with enhanced sensitivity by using regular dielectrics, without resorting to index-near-unity materials. This is enabled by the unique feature that the interfacial Cherenkov radiation is capable of controlling the sensitivity of its radiation angle to the particle velocity on demand through merely the structural design of photonic crystals.[7]

To facilitate the practical implementation of these enticing applications, it is necessary to further keep the exotic performance of interfacial Cherenkov radiation (e.g., the radiation angle) invariant to the frequency over a prescribed bandwidth. However, the interfacial Cherenkov radiation from photonic crystals is inherently chromatic. That is, its radiation angle is rather sensitive to the working frequency. This chromatic feature of interfacial Cherenkov radiation is mainly caused by the structural dispersion of photonic crystals.[38–41] This structural dispersion would persist even when the constituent materials of photonic crystals are achromatic.

Consequently, even though photonic crystals provide a versatile platform to control light–matter interactions, their structural dispersion would generally degrade the performance of directional light emission over a predefined frequency range. Current strategies to bypass the chromatic issue of photonic crystals rely heavily on numerical optimization approaches,[42–45] such as inverse design.[46–51] For example, one may mitigate the chromatic aberration of light propagation through photonic crystal fibers by carefully tailoring the structural parameters. Due to the lack of general physical insights, the extension of these numerical optimization approaches to mitigate the chromatic issue of charged particle radiation from photonic crystals is not straightforward, and indeed, this problem has remained. Altogether, despite the extensive research into both charged particle radiation[52–65] and photonic crystals,[66–76] no solution has been found to date to eliminate or at least reduce the chromatic response of charged particle radiation from photonic crystals.

Here, we reveal a feasible route to create the *achromatic* interfacial Cherenkov radiation from photonic crystals via the usage of the Brewster effect. Counterintuitively, we find that the spatially inhomogeneous photonic crystal could act like a spatially homogeneous achromatic medium (e.g., across the visible regime) for interfacial Cherenkov radiation emitted at the Brewster angle, through the judicious design of particle velocity. The underlying mechanism is essentially rooted in the anomalous Maxwell-Garnett theory, which could remain valid for photonic crystals beyond the long-wavelength limit by exploiting the Brewster effect. As background, the Maxwell-Garnett theory, dating back to the pioneering work of James Clerk Maxwell-Garnett in 1904, offers a powerful yet simple framework to describe the inhomogeneous structure as an effective homogeneous structure.[77–83] Despite its extensive research over the past century and wide applications in diverse realms, ranging from photonics, acoustics, and thermodynamics to materials science,[84–88] the Maxwell-Garnett theory has never been connected to charged particle radiation from photonic crystals. We find that the connection between Maxwell-Garnett theory and charged particle radiation from photonic crystals can significantly reduce the overall complexity in the analysis, calculation, and design of achromatic interfacial Cherenkov radiation.

RESULTS

We begin with the conceptual illustration of achromatic interfacial Cherenkov radiation from photonic crystals as shown in Fig. 1. For brevity, we consider a swift electron moving with a velocity $\bar{v} = \hat{z}v$ and traveling perpendicularly through a one-dimensional photonic crystal, which is composed of two achromatic dielectrics. The constituent dielectric X has a relative permittivity $\varepsilon_{r,X}$ and a thickness d_X, where $X = 1$ or 2. Under this scenario, the emitted light is purely p-polarized. According to the Bloch theory, the dispersion for p-polarized light inside the designed photonic crystal[89,90] is obtained as

$$\cos(k_z d) - \left[\cos(k_{z,1}d_1)\cos(k_{z,2}d_2) - \frac{1}{2}\left(\frac{\tilde{\eta}_1}{\tilde{\eta}_2} + \frac{\tilde{\eta}_2}{\tilde{\eta}_1}\right) \times \sin(k_{z,1}d_1)\sin(k_{z,2}d_2)\right] = 0, \quad (1)$$

where $\bar{k} = \hat{\perp}k_\perp + \hat{z}k_z$ is the wavevector of Bloch eigenmodes inside the photonic crystal, $\hat{\perp}$ is the basis vector perpendicular to $\hat{z}$, $d = d_1 + d_2$, $k_{z,X} = \sqrt{\frac{\omega^2}{c^2}\varepsilon_{r,X} - k_\perp^2}$, ω is the angular frequency, c is the speed of light in vacuum, and $\tilde{\eta}_X = \frac{k_{z,X}}{\omega\varepsilon_0\varepsilon_{r,X}}$ corresponds to the impedance of dielectric X under the oblique incidence of light.

Upon close inspection, Eq. (1) can be significantly reduced if $\tilde{\eta}_1 = \tilde{\eta}_2$, namely, if the impedance-matching condition is fulfilled, under which we have $k_\perp = k_{\perp,\mathrm{B}}$ and

$$k_{\perp,\mathrm{B}} = \frac{\omega}{c}\sqrt{\frac{\varepsilon_{r,1}\varepsilon_{r,2}}{\varepsilon_{r,1} + \varepsilon_{r,2}}}. \quad (2)$$

Essentially, this impedance-matching condition is related to the Brewster effect at the interface between dielectrics 1 and 2,[63,78,91–96] since the reflection coefficient at this dielectric interface is $R_{1,2} = \frac{\tilde{\eta}_1 - \tilde{\eta}_2}{\tilde{\eta}_1 + \tilde{\eta}_2} = 0$, if $\tilde{\eta}_1 = \tilde{\eta}_2$.

We now apply the impedance-matching condition into Eq. (1). To be specific, if $\tilde{\eta}_1 = \tilde{\eta}_2$, we have $\frac{1}{2}\left(\frac{\tilde{\eta}_1}{\tilde{\eta}_2} + \frac{\tilde{\eta}_2}{\tilde{\eta}_1}\right) = 1$, and Eq. (1) is reduced to $\cos(k_{z,\mathrm{B}}d) = \cos(k_{z,1}d_1 + k_{z,2}d_2)$. This way, one simple solution to Eq. (1) is $k_{z,\mathrm{B}}d = k_{z,1}d_1 + k_{z,2}d_2$. By further expressing $k_{z,X}$ with $k_{\perp,\mathrm{B}}$, this solution can be transformed to

$$\frac{k_{\perp,\mathrm{B}}^2}{\varepsilon_{\mathrm{eff},z}} + \frac{k_{z,\mathrm{B}}^2}{\varepsilon_{\mathrm{eff},\perp}} = \frac{\omega^2}{c^2}, \quad (3)$$

$$\varepsilon_{\mathrm{eff},\perp} = \frac{\varepsilon_{r,1}d_1 + \varepsilon_{r,2}d_2}{d_1 + d_2}, \quad (4)$$

$$\varepsilon_{\mathrm{eff},z} = \frac{\varepsilon_{r,1}\varepsilon_{r,2}(d_1 + d_2)}{\varepsilon_{r,1}d_2 + \varepsilon_{r,2}d_1}, \quad (5)$$

where both $\varepsilon_{\mathrm{eff},\perp}$ and $\varepsilon_{\mathrm{eff},z}$ are frequency-independent. Equations (3)–(5) indicate that the spatially inhomogeneous photonic crystal is equivalent to a spatially homogeneous achromatic uniaxial medium with an effective relative permittivity, $\bar{\bar{\varepsilon}}_r = \mathrm{diag}[\varepsilon_{\mathrm{eff},\perp}, \varepsilon_{\mathrm{eff},\perp}, \varepsilon_{\mathrm{eff},z}]$. That is, the anomalous Maxwell-Garnett theory for photonic crystals, as governed by Eqs. (3)–(5), would be valid beyond the long-wavelength limit via the Brewster effect. Despite this anomalous Maxwell-Garnett theory being reported in 1988,[78] its connection to charged particle radiation has never been explored before.

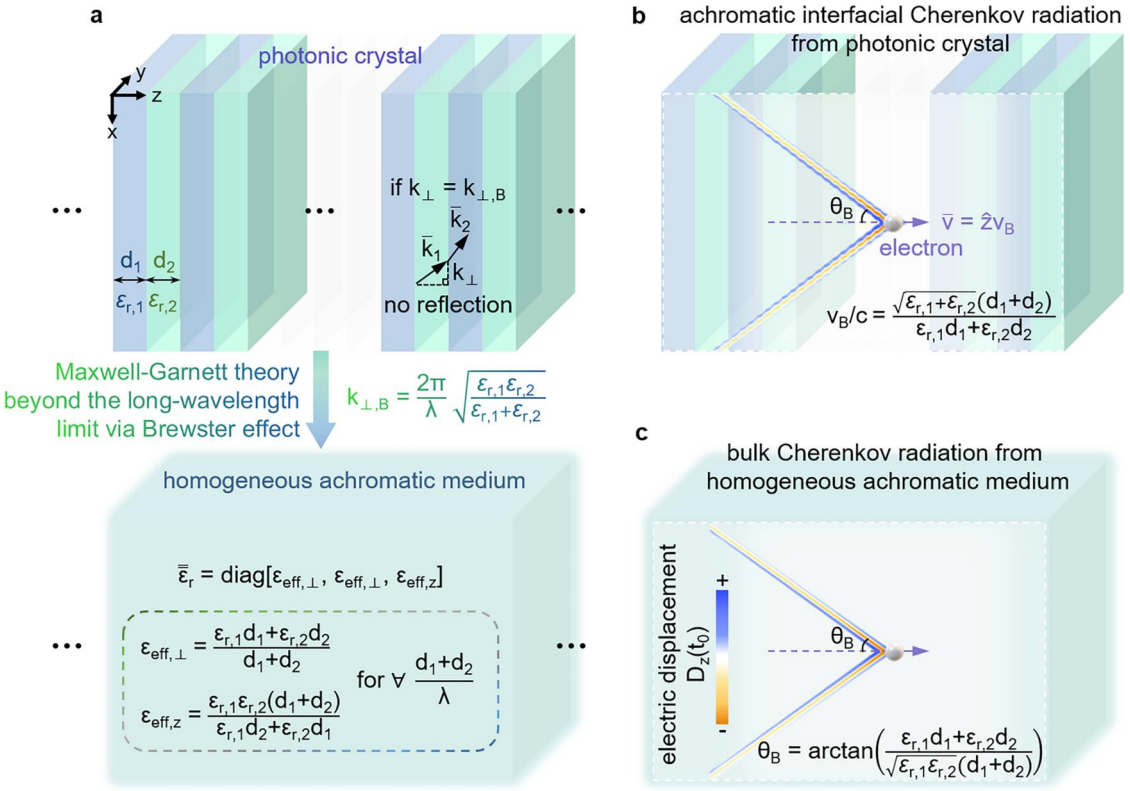

FIG. 1. Conceptual illustration of achromatic interfacial Cherenkov radiation from infinite-thickness photonic crystals. (a) Maxwell-Garnett theory beyond the long-wavelength limit via Brewster effect. The photonic crystal is composed of two achromatic dielectrics. The constituent dielectric X has a thickness d_X and a relative permittivity $\varepsilon_{r,X}$, where $X = 1$ or 2. The light inside dielectric X has a wavevector $\bar{k}_X = \hat{\perp}k_\perp + \hat{z}k_{z,X}$, where $\hat{\perp}$ is the basis vector perpendicular to $\hat{z}$. Under the incidence of light at the Brewster angle (i.e., $k_\perp = k_{\perp,B}$), there is no reflection at the dielectric interface, where $k_{\perp,B} = \frac{2\pi}{\lambda}\sqrt{\frac{\varepsilon_{r,1}\varepsilon_{r,2}}{\varepsilon_{r,1}+\varepsilon_{r,2}}}$. Under this scenario, the photonic crystal is equivalent to an achromatic medium with an effective relative permittivity $\bar{\bar{\varepsilon}}_r = \mathrm{diag}[\varepsilon_{\mathrm{eff},\perp}, \varepsilon_{\mathrm{eff},\perp}, \varepsilon_{\mathrm{eff},z}]$, where $\varepsilon_{\mathrm{eff},\perp} = \frac{\varepsilon_{r,1}d_1+\varepsilon_{r,2}d_2}{d_1+d_2}$ and $\varepsilon_{\mathrm{eff},z} = \frac{\varepsilon_{r,1}\varepsilon_{r,2}(d_1+d_2)}{\varepsilon_{r,1}d_2+\varepsilon_{r,2}d_1}$. (b) and (c) Field distribution of the electric displacement $D_z(t_0) = \int d\omega D_z(\omega)e^{-i\omega t_0}$, which is induced by a swift electron moving with a velocity $\bar{v} = \hat{z}v$ inside the photonic crystal or the effective achromatic medium. In (b) and (c), $v = v_B$ is set to ensure the emergence of achromatic interfacial Cherenkov radiation at the Brewster angle θ_B, where $v_B/c = \frac{\sqrt{\varepsilon_{r,1}+\varepsilon_{r,2}}(d_1+d_2)}{\varepsilon_{r,1}d_1+\varepsilon_{r,2}d_2}$ and $\theta_B = \arctan\left(\frac{\omega/v_B}{k_{\perp,B}}\right) = \arctan\left(\frac{\varepsilon_{r,1}d_1+\varepsilon_{r,2}d_2}{\sqrt{\varepsilon_{r,1}\varepsilon_{r,2}}(d_1+d_2)}\right)$. For illustration, here we set $\varepsilon_{r,1} = 5$, $\varepsilon_{r,2} = 2.4$, $d_1 = 150$ nm, and $d_2 = 150$ nm.

On the contrary, all Bloch eigenmodes induced by the swift electron initially have a z-component wavevector of $k_z = \omega/v$, according to the phase-matching condition along the electron moving direction (i.e., z direction). In order to create light emission at the Brewster angle θ_B inside the photonic crystal [Fig. 1(b)] or the effective uniaxial medium [Fig. 1(c)], $k_z = k_{z,B}$ is further required, namely, $\omega/v = k_{z,B}$, where $\theta_B = \arctan(k_{z,B}/k_{\perp,B})$. By substituting the condition of $k_{z,B} = \omega/v$ into Eq. (3), we have the following:

$$\frac{k_{\perp,B}^2}{\varepsilon_{\mathrm{eff},z}} + \frac{(\omega/v)^2}{\varepsilon_{\mathrm{eff},\perp}} = \frac{\omega^2}{c^2}. \tag{6}$$

From Eq. (6), the critical electron velocity that enables the emergence of achromatic interfacial Cherenkov radiation from photonic crystals [Fig. 1(b)] is obtained as $v = v_B$, where

$$v_B/c = \frac{\sqrt{\varepsilon_{r,1}+\varepsilon_{r,2}}(d_1+d_2)}{\varepsilon_{r,1}d_1+\varepsilon_{r,2}d_2}. \tag{7}$$

In practice, the photonic crystal always has finite thickness and is surrounded by the substrate and the superstrate, as schematically shown in Fig. 2(a). For illustration, we consider that both the substrate and the superstrate are composed of the same material, with a relative permittivity $\varepsilon_{r,out}$. In order to extract the excited interfacial Cherenkov radiation from the surrounding material, one necessary condition is to fulfill $|\bar{k}_{out}| \geq k_{\perp,B}$, namely, $\sqrt{\varepsilon_{r,out}} > k_{\perp,B}/(2\pi/\lambda)$, so that the total reflection at the interface between the photonic crystal and the surrounding material can be avoided, where $|\bar{k}_{out}| = (2\pi/\lambda)\sqrt{\varepsilon_{r,out}}$ is the wavevector of light in the surrounding material and $\lambda = 2\pi c/\omega$ is the wavelength of light. Since regular lossless dielectrics have a relative permittivity larger than 2,[95–97] we generally have $k_{\perp,B}/(2\pi/\lambda) = \sqrt{\frac{\varepsilon_{r,1}\varepsilon_{r,2}}{\varepsilon_{r,1}+\varepsilon_{r,2}}} > 1$, such as $k_{\perp,B}/(2\pi/\lambda) = 1.27$, if $\varepsilon_{r,1} = 5$ and $\varepsilon_{r,2} = 2.4$ are used in Fig. 2. This way, the non-vacuum surrounding material with $\sqrt{\varepsilon_{r,out}} > 1$ (e.g., $\varepsilon_{r,out} = 1.8$ used in Fig. 2) is needed in order to safely extract

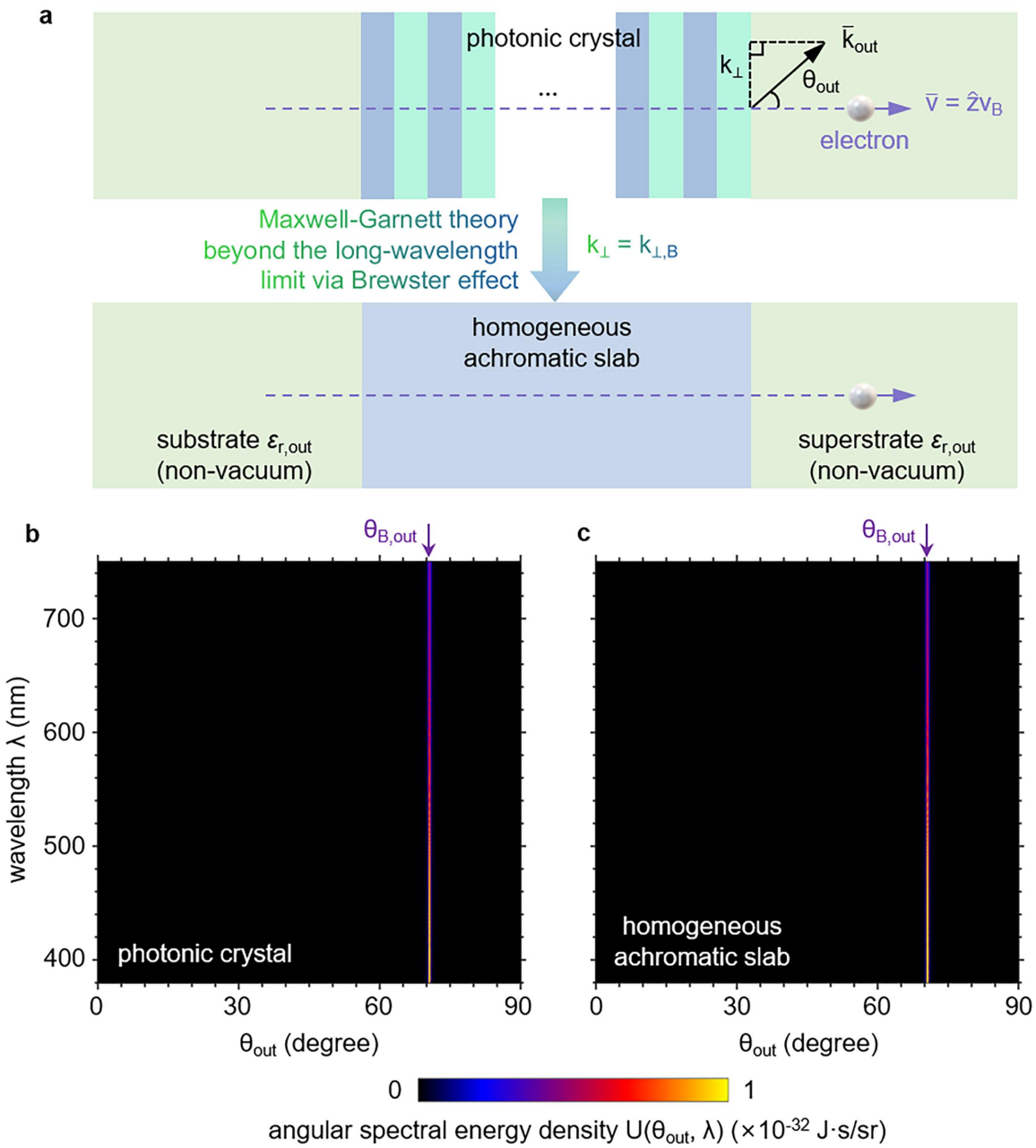

FIG. 2. Achromatic interfacial Cherenkov radiation from finite-thickness photonic crystals with non-vacuum surroundings. (a) Structural schematic. The photonic crystal and its homogenized counterpart are surrounded by the non-vacuum substrate and superstrate, both of which have a relative permittivity $\varepsilon_{r,out}$. For illustration, $\varepsilon_{r,out} = 1.8$ is used, and the photonic crystal consists of 400 unit-cells. The other setup is the same as that in Fig. 1. (b) and (c) Angular spectral energy density $U(\theta_{out}, \lambda)$ of forward light emission into the superstrate, where θ_{out} is the angle between the wavevector $\bar{k}_{out} = \hat{\perp} k_\perp + \hat{z} k_{z,out}$ of light in the superstrate and the electron velocity $\bar{v}$. The radiation peak angle $\theta_{peak}(\lambda)$ of interfacial Cherenkov radiation shows up at the Brewster angle $\theta_{B,out}$, namely, $\theta_{peak}(\lambda) = \max(U(\theta_{out}, \lambda), \theta_{out}) \equiv \theta_{B,out}$, irrespective of the working wavelength λ, where $\theta_{B,out} = \arcsin\left(\frac{k_{\perp,B}}{|\bar{k}_{out}|}\right) = \arcsin\left(\sqrt{\frac{\varepsilon_{r,1}\varepsilon_{r,2}}{(\varepsilon_{r,1}+\varepsilon_{r,2})\varepsilon_{r,out}}}\right)$ according to the Brewster effect.

the achromatic interfacial Cherenkov radiation at the Brewster angle into the surrounding material.

Under this scenario, the angular spectral energy density $U(\theta_{out}, \lambda)$ (Refs. 98–100) of the forward light emission into the superstrate is studied in Figs. 2(b) and 2(c), where θ_{out} is the angle between $\bar{k}_{out}$ and the electron velocity $\bar{v}$. When $v = v_B = 0.735c$ in Fig. 2(b), the radiation peak angle $\theta_{peak}(\lambda) = \max(U(\theta_{out}, \lambda), \theta_{out})$ always shows up at a fixed angle $\theta_{B,out}$, namely, $\theta_{peak}(\lambda) \equiv \theta_{B,out}$,

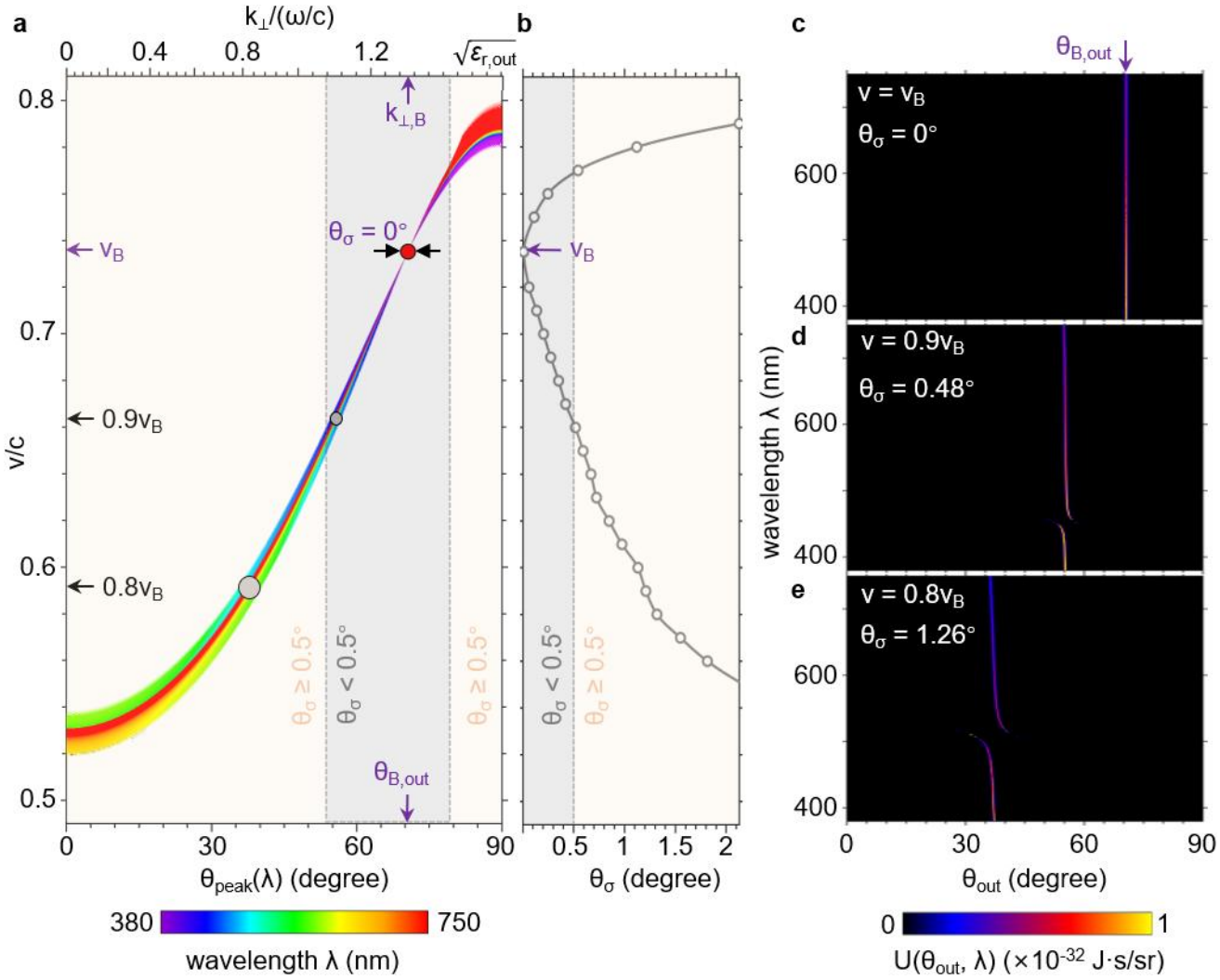

FIG. 3. Angular spread of the interfacial Cherenkov radiation from finite-thickness photonic crystals with non-vacuum surroundings. The structural setup here is the same as that in Fig. 2(a). (a) Dependence of the radiation peak angle $\theta_{peak}(\lambda)$ on the electron velocity v for various working wavelengths within the visible spectrum. The standard deviation of $\theta_{peak}(\lambda)$ throughout the visible light spectrum, namely, θ_σ, is used to quantitatively characterize the angular spread of interfacial Cherenkov radiation. (b) Dependence of the angular spread θ_σ on the electron velocity v. We have $\theta_\sigma = 0^\circ$ if $v = v_B$, where $v_B/c = 0.735$ in (a) and (b). For clarity, we argue that the achromatic interfacial Cherenkov radiation appears if $\theta_\sigma < 0.5^\circ$, e.g., in the gray regime with $v/c \in (0.661, 0.768)$, highlighted in (a) and (b). (c)–(e) Angular spectral energy density $U(\theta_{out}, \lambda)$ of forward light emission for various electron velocities.

irrespective of the working wavelength of light. This fixed angle is theoretically obtained as $\theta_{B,out} = \arcsin\left(\frac{k_{\perp,B}}{|k_{out}|}\right) = \arcsin\left(\sqrt{\frac{\varepsilon_{r,1}\varepsilon_{r,2}}{(\varepsilon_{r,1}+\varepsilon_{r,2})\varepsilon_{r,out}}}\right) = 70.6^\circ$ in Fig. 2(b), according to the phase-matching condition and the Brewster effect. Moreover, this exotic achromatic feature of interfacial Cherenkov radiation from photonic crystals in Fig. 2(b) is the same as that of bulk Cherenkov radiation from the effective achromatic uniaxial medium in Fig. 2(c).

Figure 3 further investigates the angular spread of interfacial Cherenkov radiation from finite-thickness photonic crystals with non-vacuum surroundings. Without loss of generality, the standard deviation of the radiation peak angle $\theta_{peak}(\lambda)$ throughout the whole visible spectrum, namely, θ_σ, is used to quantitatively characterize the chromatic feature (e.g., the angular spread) of interfacial Cherenkov radiation from photonic crystals in Figs. 3(a) and 3(b). When the electron velocity v is equal to the critical velocity v_B, namely, $v = v_B = 0.735c$ in Fig. 3(c), we have $\theta_{peak}(\lambda) \equiv \theta_{B,out}$ and $\theta_\sigma = 0^\circ$ throughout the visible spectrum in Figs. 3(a) and 3(b). When the electron velocity slightly deviates from the critical velocity [e.g., $v = 0.9v_B$ in Fig. 3(d)], the angular spread θ_σ is quite small and relatively insensitive to the variation of electron velocity in Figs. 3(a) and 3(b). To be specific, we have $\theta_\sigma < 0.5^\circ$, if $v/c \in (0.661, 0.768)$ in Fig. 3(b). When the electron velocity further deviates from the critical velocity [e.g., $v = 0.8v_B$ in Fig. 3(e)], the

angular spread θ_σ would increase rapidly and become sensitive to the variation of electron velocity in Figs. 3(a) and 3(b).

For conceptual demonstration, below we define that the achromatic interfacial Cherenkov radiation appears within a prescribed wavelength regime if $\theta_\sigma < 0.5^\circ$. The robustness of achromatic interfacial Cherenkov radiation with respect to the electron velocity in Fig. 3 is essentially related to the robustness of the anomalous Maxwell-Garnett theory with respect to the impedance-matching condition $\tilde{\eta}_1 = \tilde{\eta}_2$. To be specific, if the impedances of two constituent dielectrics have $\tilde{\eta}_1 \approx \tilde{\eta}_2$, instead of $\tilde{\eta}_1 = \tilde{\eta}_2$, we have the factor $\frac{1}{2}\left(\frac{\tilde{\eta}_1}{\tilde{\eta}_2} + \frac{\tilde{\eta}_2}{\tilde{\eta}_1}\right) \approx 1$ in Eq. (1), which can still be approximately reorganized into Eqs. (3)–(5). On this basis, the dependence of the peak angle of interfacial Cherenkov radiation on the electron velocity, as governed by the anomalous Maxwell-Garnett theory, can remain valid if the impedance-matching condition is approximately fulfilled or if $v \approx v_B$ (see also the supplementary material for more details).

We now proceed to discuss the possibility of achieving achromatic interfacial Cherenkov radiation from finite-thickness photonic crystals with vacuum surrounding in Figs. 4(a)–4(c). This issue is of practical importance, since the detection of interfacial Cherenkov radiation in vacuum surroundings would generally be much more convenient than that in non-vacuum surroundings. However, when the electron velocity is equal to the critical velocity, the achromatic interfacial Cherenkov radiation emitted at the Brewster angle inside the photonic crystal with $\theta_\sigma = 0^\circ$ has $k_\perp = k_{\perp,B} > 2\pi/\lambda$ and cannot couple into the vacuum surrounding due to the total reflection at the interface between the photonic crystal and vacuum. As a result, the forward light emission into the vacuum superstrate will not contain the signal of achromatic interfacial Cherenkov radiation and is of poor directionality and intensity in Fig. 4(b). On the contrary, when the electron velocity is smaller than the critical velocity and judiciously designed, the achromatic interfacial Cherenkov radiation emitted at the non-Brewster angle with $\theta_\sigma < 0.5^\circ$ can have $k_\perp < 2\pi/\lambda < k_{\perp,B}$; see Fig. 3(a) for example. This indicates an enticing scheme to get rid of the total reflection at the interface between the photonic crystal and the vacuum and to safely extract the achromatic interfacial Cherenkov radiation into the vacuum surrounding. For example, when $\varepsilon_{r,1} = 2.18$ [e.g., SiO_2

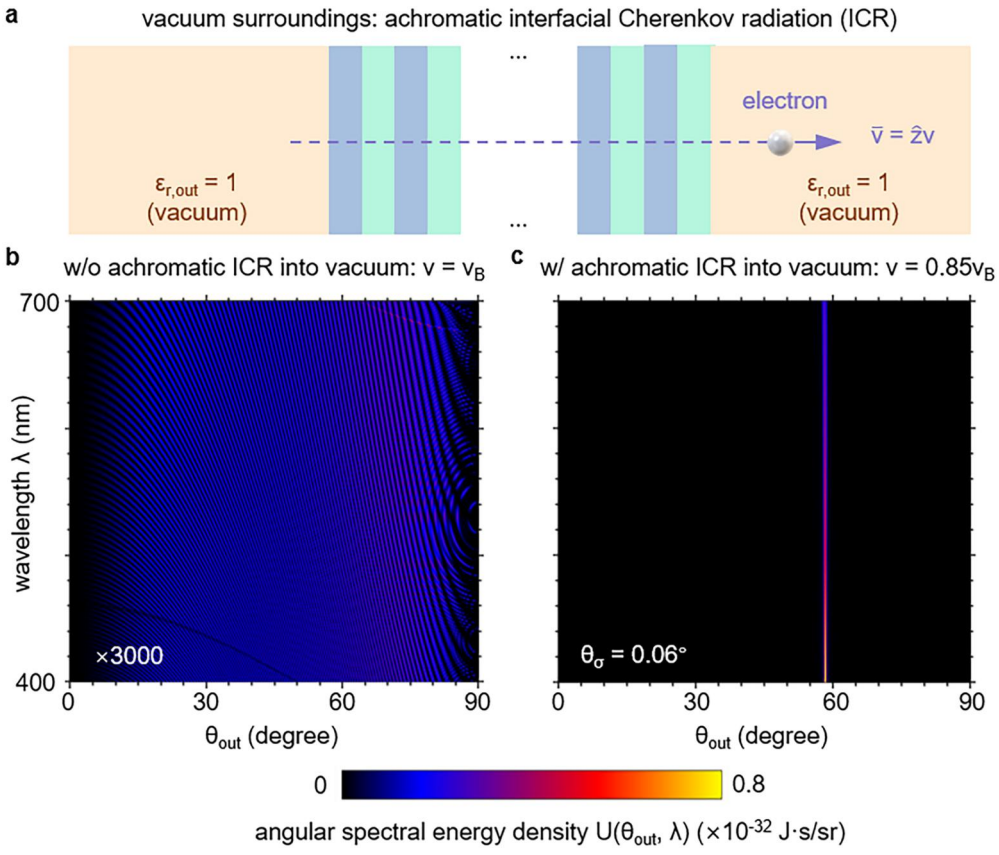

FIG. 4. Achromatic interfacial Cherenkov radiation from finite-thickness photonic crystals with vacuum surroundings. (a) Structural schematic. Both the substrate and superstrate are vacuum. For illustration, here we set $\varepsilon_{r,1} = 2.18$ [e.g., SiO_2 (Ref. 101)] and $\varepsilon_{r,2} = 2.56$ [e.g., LaF_3 (Ref. 102)]. The other structural setup is the same as that in Fig. 2. (b) and (c) Angular spectral energy density $U(\theta_{out}, \lambda)$ of forward light emission for different electron velocities. If $v = v_B$ in (b), due to the total internal reflection at the interface between vacuum and the photonic crystal, the achromatic interfacial Cherenkov radiation created inside the photonic crystal with $k_\perp = k_{\perp,B} > 2\pi/\lambda$ cannot couple into vacuum, where $k_{\perp,B}/(2\pi/\lambda) = \sqrt{\frac{\varepsilon_{r,1}\varepsilon_{r,2}}{\varepsilon_{r,1}+\varepsilon_{r,2}}} = 1.09$ and $v_B/c = 0.919$. If $v \neq v_B$ (e.g., $v = 0.85v_B$) in (c), the achromatic interfacial Cherenkov radiation created inside the photonic crystal with $k_\perp < 2\pi/\lambda < k_{\perp,B}$ [e.g., $k_\perp/(2\pi/\lambda) = 0.85$ in (c)] can couple into vacuum.

(Ref. 101)], $\varepsilon_{r,2} = 2.56$ [e.g., LaF_3 (Ref. 102)], and $v = 0.85v_B$ in Fig. 4(c), the achromatic interfacial Cherenkov radiation with $\theta_\sigma = 0.06^\circ$ shows up in the vacuum superstrate.

DISCUSSION

In conclusion, we have unveiled the enticing possibility of creating achromatic interfacial Cherenkov radiation from photonic crystals via the Brewster effect. According to the anomalous Maxwell-Garnett theory beyond the long-wavelength limit, we have found that the photonic crystal is essentially equivalent to a homogeneous achromatic medium for achromatic interfacial Cherenkov radiation emitted at the Brewster angle. This finding indicates a brand-new paradigm to deal with the chromatic issues in complex photonic systems and should be of fundamental importance to facilitate the development of charged particle-driven achromatic optical devices (e.g., miniaturized achromatic photonic Cherenkov detectors for the identification of high-energy particles with improved sensitivity), which are crucial to many practical applications, including communications, on-chip information processing, biomedical sensing, chemical detection, and imaging. This finding also indicates rich unexplored physics still exists in the realm of light–particle–matter interactions and might stimulate continuous explorations of achromatic light emission and scattering (including charged particle radiation) from more sophisticated but exotic optical systems,[103–105] such as random media and spatiotemporal media. Particularly, whether we can realize the achromatic charged particle radiation with high directionality from random media (e.g., via the extension of the anomalous Maxwell-Garnett theory to random media) remains elusive and is certainly worthy of further in-depth investigation.

SUPPLEMENTARY MATERIAL

See the supplementary material for the three sections, including derivation of interfacial Cherenkov radiation from photonic crystals, derivation of conventional bulk Cherenkov radiation from the effective homogeneous achromatic uniaxial slab, and more discussion on achromatic interfacial Cherenkov radiation from photonic crystals.

ACKNOWLEDGMENTS

X.L. acknowledges the support partly from the National Natural Science Foundation of China (NSFC) (Grant Nos. W2543013 and 62475227), the National Key Research and Development Program of China (Grant No. 2025YFF0514901), and the Zhejiang Provincial Natural Science Foundation of China (Grant No. LR26F050002). H.C. acknowledges the support from the Key Research and Development Program of the Ministry of Science and Technology (Grant Nos. 2022YFA1404704 and 2022YFA1405201) and NSFC (Grant Nos. U25A20520 and 62475228). O.M. acknowledges support by the Simons Collaboration on Extreme Wave Phenomena Based on Symmetries (Award No. SFI-MPS-EWP-00008530-09). The authors dedicate this work to the memory of Professor John Joannopoulos, honoring his pioneering contributions to the launch of modern nanophotonics and his personal mentorship.

AUTHOR DECLARATIONS

Conflict of Interest

The authors have no conflicts to disclose.

Author Contributions

Xiangfeng Xi and Zheng Gong contributed equally to this paper.

Xiangfeng Xi: Conceptualization (equal); Data curation (equal); Formal analysis (equal); Investigation (equal); Methodology (equal); Resources (equal); Validation (equal); Visualization (equal); Writing – original draft (equal); Writing – review & editing (equal). **Zheng Gong:** Conceptualization (equal); Methodology (equal); Validation (equal); Visualization (equal); Writing – original draft (equal); Writing – review & editing (equal). **Ruoxi Chen:** Funding acquisition (equal); Writing – review & editing (supporting). **Zun Wang:** Writing – review & editing (supporting). **Owen D. Miller:** Funding acquisition (equal); Supervision (supporting); Writing – review & editing (supporting). **Yi Yang:** Supervision (supporting); Writing – review & editing (supporting). **Hongsheng Chen:** Funding acquisition (equal); Supervision (supporting); Writing – review & editing (supporting). **Ido Kaminer:** Supervision (supporting); Writing – review & editing (supporting). **Xiao Lin:** Conceptualization (equal); Formal analysis (equal); Funding acquisition (lead); Investigation (equal); Methodology (equal); Project administration (lead); Supervision (equal); Validation (equal); Visualization (equal); Writing – original draft (equal); Writing – review & editing (lead).

DATA AVAILABILITY

The data that support the findings of this study are available within the article and its supplementary material.

REFERENCES

[1]P. A. Cherenkov, "Radiation from high-speed particles," Science **131**, 136–142 (1960).
[2]I. M. Frank, "Optics of light sources moving in refractive media," Science **131**, 702–712 (1960).
[3]I. E. Tamm, "General characteristics of Vavilov-Cherenkov radiation," Science **131**, 206–210 (1960).
[4]IceCube Collaboration *et al.*, "Observation of high-energy neutrinos from the Galactic plane," Science **380**, 1338–1343 (2023).
[5]P. Padovani, E. Resconi, M. Ajello, C. Bellenghi, S. Bianchi, P. Blasi, K.-Y. Huang, S. Gabici, V. Gámez Rosas, H. Niederhausen, E. Peretti, B. Eichmann, D. Guetta, A. Lamastra, and T. Shimizu, "High-energy neutrinos from the vicinity of the supermassive black hole in NGC 1068," Nat. Astron. **8**, 1077–1087 (2024).
[6]X. Lin, H. Hu, S. Easo, Y. Yang, Y. Shen, K. Yin, M. P. Blago, I. Kaminer, B. Zhang, H. Chen, J. Joannopoulos, M. Soljačić, and Y. Luo, "A Brewster route to Cherenkov detectors," Nat. Commun. **12**, 5554 (2021).
[7]X. Lin, S. Easo, Y. Shen, H. Chen, B. Zhang, J. D. Joannopoulos, M. Soljačić, and I. Kaminer, "Controlling Cherenkov angles with resonance transition radiation," Nat. Phys. **14**, 816–821 (2018).
[8]H. Hu, X. Lin, L. J. Wong, Q. Yang, D. Liu, B. Zhang, and Y. Luo, "Surface Dyakonov-Cherenkov radiation," eLight **2**(1), 2 (2022).
[9]Y.-F. Li, R. Shaisultanov, K. Z. Hatsagortsyan, F. Wan, C. H. Keitel, and J.-X. Li, "Ultrarelativistic electron-beam polarization in single-shot interaction with an ultraintense laser pulse," Phys. Rev. Lett. **122**, 154801 (2019).
[10]C. Roques-Carmes, S. E. Kooi, Y. Yang, N. Rivera, P. D. Keathley, J. D. Joannopoulos, S. G. Johnson, I. Kaminer, K. K. Berggren, and M. Soljačić, "Free-electron-light interactions in nanophotonics," Appl. Phys. Rev. **10**, 011303 (2023).
[11]Y. Yang, C. Roques-Carmes, S. E. Kooi, H. Tang, J. Beroz, E. Mazur, I. Kaminer, J. D. Joannopoulos, and M. Soljaić, "Photonic flatband resonances for free-electron radiation," Nature **613**, 42–47 (2023).
[12]F. Liu, L. Xiao, Y. Ye, M. Wang, K. Cui, X. Feng, W. Zhang, and Y. Huang, "Integrated Cherenkov radiation emitter eliminating the electron velocity threshold," Nat. Photonics **11**, 289–292 (2017).

[13]H. Hu, X. Lin, and Y. Luo, "Free-electron radiation engineering via structured environments," Prog. Electromagn. Res. **171**, 75–88 (2021).
[14]Z. Xie, Z. Chen, H. Li, Q. Yan, H. Chen, X. Lin, I. Kaminer, O. D. Miller, and Y. Yang, "Maximal quantum interaction between free electrons and photons," Phys. Rev. Lett. **134**, 043803 (2025).
[15]Y. Adiv, H. Hu, S. Tsesses, R. Dahan, K. Wang, Y. Kurman, A. Gorlach, H. Chen, X. Lin, G. Bartal, and I. Kaminer, "Observation of 2D Cherenkov radiation," Phys. Rev. X **13**, 011002 (2023).
[16]F. Tay, X. Lin, X. Shi, H. Chen, I. Kaminer, and B. ZhangTay, "Bulk-plasmon-mediated free-electron radiation beyond the conventional formation time," Adv. Sci. **10**, 2300760 (2023).
[17]D. Pan and H. Xu, "Polarizing free electrons in optical near fields," Phys. Rev. Lett. **130**, 186901 (2023).
[18]N. Pramanik, S. Huang, R. Duan, Q. Zhai, M. Go, C. Boothroyd, Z. Liu, and L. J. Wong, "Fundamental scaling laws of water-window x-rays from free-electron-driven van der Waals structures," Nat. Photonics **18**, 1203–1211 (2024).
[19]X. Lin and H. Chen, "Shaping free-electron radiation via van der Waals heterostructures," Light: Sci. Appl. **12**, 187 (2023).
[20]T. Bucher, H. Nahari, H. Herzig Sheinfux, R. Ruimy, A. Niedermayr, R. Dahan, Q. Yan, Y. Adiv, M. Yannai, J. Chen, Y. Kurman, S. Tae Park, D. J. Masiel, E. Janzen, J. H. Edgar, F. Carbone, G. Bartal, S. Tsesses, F. H. L. Koppens, G. M. Vanacore, and I. Kaminer, "Coherently amplified ultrafast imaging using a free-electron interferometer," Nat. Photonics **18**, 809–815 (2024).
[21]J. H. Gaida, H. Lourenço-Martins, M. Sivis, T. Rittmann, A. Feist, F. J. García de Abajo, and C. Ropers, "Attosecond electron microscopy by free-electron homodyne detection," Nat. Photonics **18**, 509–515 (2024).
[22]D. A. Alexander, A. Nomezine, L. A. Jarvis, D. J. Gladstone, B. W. Pogue, and P. Bruza, "Color Cherenkov imaging of clinical radiation therapy," Light: Sci. Appl. **10**, 226 (2021).
[23]Y. Chen, K. Zeng, Z. Xie, Y. Sha, Z. Chen, X. Zhang, S. Yang, S. Gong, Y. Chen, H. Duan, S. Zhang, and Y. Yang, "Synthetic gain for electron-beam spectroscopy," arXiv:2410.16989 (2024).
[24]A. K. Glaser, R. Zhang, J. M. Andreozzi, D. J. Gladstone, and B. W. Pogue, "Cherenkov radiation fluence estimates in tissue for molecular imaging and therapy applications," Phys. Med. Biol. **60**, 6701 (2015).
[25]T. M. Shaffer, E. C. Pratt, and J. Grimm, "Utilizing the power of Cerenkov light with nanotechnology," Nat. Nanotechnol. **12**, 106–117 (2017).
[26]N. L. Streshkova, P. Koutenský, T. Novotný, and M. Kozák, "Monochromatization of electron beams with spatially and temporally modulated optical fields," Phys. Rev. Lett. **133**, 213801 (2024).
[27]Z. Duan, X. Tang, Z. Wang, Y. Zhang, X. Chen, M. Chen, and Y. Gong, "Observation of the reversed Cherenkov radiation," Nat. Commun. **8**, 14901 (2017).
[28]M. Adinolfi *et al.*, "Performance of the LHCb RICH detector at the LHC," Eur. Phys. J. C **73**, 2431 (2013).
[29]Z. Gong, J. Chen, R. Chen, X. Zhu, C. Wang, X. Zhang, H. Hu, Y. Yang, B. Zhang, H. Chen, I. Kaminer, and X. Lin, "Interfacial Cherenkov radiation from ultralow-energy electrons," Proc. Natl. Acad. Sci. U. S. A. **120**, e2306601120 (2023).
[30]G. Adamo, K. F. MacDonald, Y. H. Fu, C.-M. Wang, D. P. Tsai, F. J. García de Abajo, and N. I. Zheludev, "Light well: A tunable free-electron light source on a chip," Phys. Rev. Lett. **103**, 113901 (2009).
[31]J.-W. Henke, A. S. Raja, A. Feist, G. Huang, G. Arend, Y. Yang, F. J. Kappert, R. N. Wang, M. Möller, and J. Pan, "Integrated photonics enables continuous-beam electron phase modulation," Nature **600**, 653–658 (2021).
[32]Y. Yang, J.-W. Henke, A. S. Raja, F. J. Kappert, G. Huang, G. Arend, Z. Qiu, A. Feist, R. N. Wang, A. Tusnin, A. Tikan, C. Ropers, and T. J. Kippenberg, "Free-electron interaction with nonlinear optical states in microresonators," Science **383**, 168–173 (2024).
[33]A. Feist, G. Huang, G. Arend, Y. Yang, J.-W. Henke, A. S. Raja, F. J. Kappert, R. N. Wang, H. Lourenço-Martins, Z. Qiu, J. Liu, O. Kfir, T. J. Kippenberg, and C. Ropers, "Cavity-mediated electron-photon pairs," Science **377**, 777–780 (2022).
[34]C. Roques-Carmes *et al.*, "Towards integrated tunable all-silicon free-electron light sources," Nat. Commun. **10**, 3176 (2019).
[35]E. Prat, A. Al Haddad, C. Arrell, S. Augustin, M. Boll, C. Bostedt, M. Calvi, A. L. Cavalieri, P. Craievich, A. Dax, P. Dijkstal, E. Ferrari, R. Follath, R. Ganter, Z. Geng, N. Hiller, M. Huppert, R. Ischebeck, P. Juranić, C. Kittel, G. Knopp, A. Malyzhenkov, F. Marcellini, S. Neppl, S. Reiche, N. Sammut, T. Schietinger, T. Schmidt, K. Schnorr, A. Trisorio, C. Vicario, D. Voulot, G. Wang, and T. Weilbach, "An x-ray free-electron laser with a highly configurable undulator and integrated chicanes for tailored pulse properties," Nat. Commun. **14**, 5069 (2023).
[36]G. Perosa, J. Wätzel, D. Garzella, E. Allaria, M. Bonanomi, M. B. Danailov, A. Brynes, C. Callegari, G. De Ninno, A. Demidovich, M. D. Fraia, S. D. Mitri, L. Giannessi, M. Manfredda, L. Novinec, N. Pal, G. Penco, O. Plekan, K. C. Prince, A. Simoncig, S. Spampinati, C. Spezzani, M. Zangrando, J. Berakdar, R. Feifel, R. J. Squibb, R. Coffee, E. Hemsing, E. Roussel, G. Sansone, B. W. J. McNeil, and P. R. Ribič, "Femtosecond polarization shaping of free-electron laser pulses," Phys. Rev. Lett. **131**, 045001 (2023).
[37]P. Franz, S. Li, T. Driver, R. R. Robles, D. Cesar, E. Isele, Z. Guo, J. Wang, J. P. Duris, K. Larsen, J. M. Glownia, X. Cheng, M. C. Hoffmann, X. Li, M.-F. Lin, A. Kamalov, R. Obaid, A. Summers, N. Sudar, E. Thierstein, Z. Zhang, M. F. Kling, Z. Huang, J. P. Cryan, and A. Marinelli, "Terawatt-scale attosecond x-ray pulses from a cascaded superradiant free-electron laser," Nat. Photonics **18**, 698–703 (2024).
[38]J. D. Joannopoulos, S. G. Johnson, J. N. Winn, and R. D. Meade, *Photonic Crystals: Molding the Flow of Light* (Princeton University Press, 2008).
[39]T. Baba, "Slow light in photonic crystals," Nat. Photonics **2**, 465–473 (2008).
[40]Z. V. Vardeny, A. Nahata, and A. Agrawal, "Optics of photonic quasicrystals," Nat. Photonics **7**, 177–187 (2013).
[41]G.-J. Tang, X.-T. He, F.-L. Shi, J.-W. Liu, X.-D. Chen, and J.-W. Dong, "Topological photonic crystals: Physics, designs, and applications," Laser Photonics Rev. **16**, 2100300 (2022).
[42]W. H. Reeves, D. V. Skryabin, F. Biancalana, J. C. Knight, P. S. J. Russell, F. G. Omenetto, A. Efimov, and A. J. Taylor, "Transformation and control of ultra-short pulses in dispersion-engineered photonic crystal fibres," Nature **424**, 511–515 (2003).
[43]X. Ni, Y. Liu, B. Lou, M. Zhang, E. L. Hu, S. Fan, E. Mazur, and H. Tang, "Three-dimensional reconfigurable optical singularities in bilayer photonic crystals," Phys. Rev. Lett. **132**, 073804 (2024).
[44]S.-C. Jiang, X. Xiong, Y.-S. Hu, Y.-H. Hu, G.-B. Ma, R.-W. Peng, C. Sun, and M. Wang, "Controlling the polarization state of light with a dispersion-free metastructure," Phys. Rev. X **4**, 021026 (2014).
[45]X.-C. Ai, S.-C. Pan, Y.-H. Wang, and S.-C. Tian, "Optimization design of photonic-crystal surface-emitting lasers: Toward large bandwidth and single-lane 200G optical transmission," Prog. Electromagn. Res. **180**, 89–101 (2024).
[46]L. Norder, S. Yin, M. H. J. de Jong, F. Stallone, H. Aydogmus, P. M. Sberna, M. A. Bessa, and R. A. Norte, "Pentagonal photonic crystal mirrors: Scalable lightsails with enhanced acceleration via neural topology optimization," Nat. Commun. **16**, 2753 (2025).
[47]S. Molesky, Z. Lin, A. Y. Piggott, W. Jin, J. Vucković, and A. W. Rodriguez, "Inverse design in nanophotonics," Nat. Photonics **12**, 659–670 (2018).
[48]T. B. Kanmaz, E. Ozturk, H. V. Demir, and C. Gunduz-Demir, "Deep-learning-enabled electromagnetic near-field prediction and inverse design of metasurfaces," Optica **10**, 1373–1382 (2023).
[49]E. Lucas, S.-P. Yu, T. C. Briles, D. R. Carlson, and S. B. Papp, "Tailoring microcombs with inverse-designed, meta-dispersion microresonators," Nat. Photonics **17**, 943–950 (2023).
[50]V. Nikkhah, A. Pirmoradi, F. Ashtiani, B. Edwards, F. Aflatouni, and N. Engheta, "Inverse-designed low-index-contrast structures on a silicon photonics platform for vector-matrix multiplication," Nat. Photonics **18**, 501–508 (2024).
[51]Z. Li, S. Ma, S. Li, O. You, Y. Liu, Q. Yang, Y. Xiang, P. Zhou, and S. Zhang, "Observation of copropagating chiral zero modes in magnetic photonic crystals," Phys. Rev. Lett. **134**, 033802 (2025).
[52]C. Pellegrini, A. Marinelli, and S. Reiche, "The physics of x-ray free-electron lasers," Rev. Mod. Phys. **88**, 015006 (2016).
[53]A. Gonoskov, T. Blackburn, M. Marklund, and S. Bulanov, "Charged particle motion and radiation in strong electromagnetic fields," Rev. Mod. Phys. **94**, 045001 (2022).

[54]R. Chen, Z. Gong, Z. Wang, X. Xi, B. Zhang, Y. Yang, B. Zhang, I. Kaminer, H. Chen, and X. Lin, "A gain route to reversed Cherenkov radiation," Sci. Adv. **11**, eads5113 (2025).
[55]J. Chen, R. Chen, F. Tay, Z. Gong, H. Hu, Y. Yang, X. Zhang, C. Wang, I. Kaminer, H. Chen, B. Zhang, and X. Lin, "Low-velocity-favored transition radiation," Phys. Rev. Lett. **131**, 113002 (2023).
[56]L. Jing, X. Lin, Z. Wang, I. Kaminer, H. Hu, E. Li, Y. Liu, M. Chen, B. Zhang, and H. Chen, "Polarization shaping of free-electron radiation by gradient bianisotropic metasurfaces," Laser Photonics Rev. **15**, 2000426 (2021).
[57]X. Lin, I. Kaminer, X. Shi, F. Gao, Z. Yang, Z. Gao, H. Buljan, J. D. Joannopoulos, M. Soljačić, H. Chen, and B. Zhang, "Splashing transients of 2D plasmons launched by swift electrons," Sci. Adv. **3**, e1601192 (2017).
[58]J. Chen, H. Chen, and X. Lin, "Photonic and plasmonic transition radiation from graphene," J. Opt. **23**, 034001 (2021).
[59]Z. Zhao, "Upper bound for the quantum coupling between free electrons and photons," Phys. Rev. Lett. **134**, 043804 (2025).
[60]A. Preimesberger, D. Hornof, T. Dorfner, T. Schachinger, M. Hrtoň, A. Konečná, and P. Haslinger, "Exploring single-photon recoil on free electrons," Phys. Rev. Lett. **134**, 096901 (2025).
[61]S. Huang, R. Duan, N. Pramanik, J. S. Herrin, C. Boothroyd, Z. Liu, and L. J. Wong, "Quantum recoil in free-electron interactions with atomic lattices," Nat. Photonics **17**, 224–230 (2023).
[62]J. Zhang, H. Cui, Y. Liu, X. Zhang, Y. Li, D. Zhao, Y. Zhao, and Q. Zhan, "Producing focused extreme ultraviolet vortex with Fermat-spiral photon sieves," PhotoniX **5**, 15 (2024).
[63]Z. Gong, R. Chen, Z. Wang, X. Xi, Y. Yang, B. Zhang, H. Chen, I. Kaminer, and X. Lin, "Free-electron resonance transition radiation via Brewster randomness," Proc. Natl. Acad. Sci. U. S. A. **122**, e2413336122 (2025).
[64]Z. Wang, Z. Gong, R. Chen, X. Xi, J. Chen, Y. Yang, H. Chen, E. Li, I. Kaminer, and X. Lin, "Ultra-directional transition radiation from deep-subwavelength epsilon-near-zero metamaterials," Adv. Opt. Mater. **14**, e01449 (2026).
[65]B. Zhang, Z. Gong, R. Chen, X. Chen, Y. Yang, H. Chen, I. Kaminer, and X. Lin, "Reversed Cherenkov radiation via Fizeau-Fresnel drag," Appl. Phys. Rev. **12**, 041421 (2025).
[66]Y. Wang, H.-X. Wang, L. Liang, W. Zhu, L. Fan, Z.-K. Lin, F. Li, X. Zhang, P.-G. Luan, Y. Poo, J.-H. Jiang, and G.-Y. Guo, "Hybrid topological photonic crystals," Nat. Commun. **14**, 4457 (2023).
[67]G. Posnjak, X. Yin, P. Butler, O. Bienek, M. Dass, S. Lee, I. D. Sharp, and T. Liedl, "Diamond-lattice photonic crystals assembled from DNA origami," Science **384**, 781–785 (2024).
[68]H. Qin, Z. Su, Z. Zhang, W. Lv, Z. Yang, W. Chen, X. Gao, H. Wei, Y. Shi, B. Li, J. Zhou, R. Fleury, C.-W. Qiu, and Q. Song, "Disorder-assisted real-momentum topological photonic crystal," Nature **639**, 602–608 (2025).
[69]M. C. Rechtsman, "Reciprocal topological photonic crystals allow backscattering," Nat. Photonics **17**, 383–384 (2023).
[70]Z. Sun, L. Cao, L. Wang, W. Wu, H. Yang, J. Wang, W. Luo, M. Ren, W. Cai, and J. Xu, "Smith-Purcell radiation in two dimensions," Phys. Rev. Lett. **134**, 043802 (2025).
[71]L. W. W. Wong, X. Shi, A. Karnieli, J. Lim, S. Kumar, S. Carbajo, I. Kaminer, and L. J. Wong, "Free-electron crystals for enhanced x-ray radiation," Light: Sci. Appl. **13**, 29 (2024).
[72]R. Barczyk, L. Kuipers, and E. Verhagen, "Observation of Landau levels and chiral edge states in photonic crystals through pseudomagnetic fields induced by synthetic strain," Nat. Photonics **18**, 574–579 (2024).
[73]X.-X. Wang, Z. Guo, J. Song, H. Jiang, H. Chen, and X. Hu, "Unique Huygens-Fresnel electromagnetic transportation of chiral Dirac wavelet in topological photonic crystal," Nat. Commun. **14**, 3040 (2023).
[74]Y. Xie, M. Khalil, H. Sun, J. Liu, Z. Lu, P. J. Poole, J. Weber, G. Liu, M. Rahim, and L. R. Chen, "Applications of quantum dash mode-locked laser in microwave photonics," Electromagn. Sci. **3**, 0090271 (2025).
[75]J. Luo, Y. Yang, Z. Yao, W. Lu, B. Hou, Z. H. Hang, C. T. Chan, and Y. Lai, "Ultratransparent media and transformation optics with shifted spatial dispersions," Phys. Rev. Lett. **117**, 223901 (2016).
[76]T. Song, H. Chu, J. Luo, Z. Cao, M. Xiao, R. Peng, M. Wang, and Y. Lai, "Ultracompact photonic circuits without cladding layers," Phys. Rev. X **12**, 011053 (2022).
[77]G. J. Maxwell and B. Garnett, "Colours in metal glasses and in metallic films," Philos. Trans. R. Soc., A **203**, 385–420 (1904).
[78]J. E. Sipe, P. Sheng, B. S. White, and M. H. Cohen, "Brewster anomalies: A polarization-induced delocalization effect," Phys. Rev. Lett. **60**, 108 (1988).
[79]D. R. Smith, S. Schultz, P. Markoš, and C. M. Soukoulis, "Determination of effective permittivity and permeability of metamaterials from reflection and transmission coefficients," Phys. Rev. B **65**, 195104 (2002).
[80]W. Cai and V. Shalaev, *Optical Metamaterials: Fundamentals and Applications* (Springer, New York, 2010).
[81]C. Rizza and A. Ciattoni, "Effective medium theory for Kapitza stratified media: Diffractionless propagation," Phys. Rev. Lett. **110**, 143901 (2013).
[82]H. Herzig Sheinfux, I. Kaminer, Y. Plotnik, G. Bartal, and M. Segev, "Subwavelength multilayer dielectrics: Ultrasensitive transmission and breakdown of effective-medium theory," Phys. Rev. Lett. **113**, 243901 (2014).
[83]S. Yuan, X. Zhou, Y. Chen, Y. Zhong, L. Sheng, H. Hu, H. Chen, I. Kaminer, and X. Lin, "Breakdown of effective-medium theory by a photonic spin Hall effect," Sci. China Phys. Mech. Astron. **66**, 114212 (2023).
[84]Z. Gong, R. Chen, H. Chen, and X. Lin, "Anomalous Maxwell-Garnett theory for photonic time crystals," Appl. Phys. Rev. **12**, 031414 (2025).
[85]P. A. Huidobro, M. G. Silveirinha, E. Galiffi, and J. Pendry, "Homogenization theory of space-time metamaterials," Phys. Rev. Appl. **16**, 014044 (2021).
[86]Y. Sharabi, A. Dikopoltsev, E. Lustig, Y. Lumer, and M. Segev, "Spatiotemporal photonic crystals," Optica **9**, 585–592 (2022).
[87]S. Safaei Jazi, I. Faniayeu, R. Cichelero, D. C. Tzarouchis, M. M. Asgari, A. Dmitriev, S. Fan, and V. Asadchy, "Optical Tellegen metamaterial with spontaneous magnetization," Nat. Commun. **15**, 1293 (2024).
[88]N. Engheta, "Four-dimensional optics using time-varying metamaterials," Science **379**, 1190–1191 (2023).
[89]Z. Zhang and S. Satpathy, "Electromagnetic wave propagation in periodic structures: Bloch wave solution of Maxwell's equations," Phys. Rev. Lett. **65**, 2650 (1990).
[90]B. Wood, J. Pendry, and D. Tsai, "Directed subwavelength imaging using a layered metal-dielectric system," Phys. Rev. **74**, 115116 (2006).
[91]R. Paniagua-Domínguez, Y. F. Yu, A. E. Miroshnichenko, L. A. Krivitsky, Y. H. Fu, V. Valuckas, L. Gonzaga, Y. T. Toh, A. Y. S. Kay, B. Luk'yanchuk, and A. I. Kuznetsov, "Generalized Brewster effect in dielectric metasurfaces," Nat. Commun. **7**, 10362 (2016).
[92]X. Lin, Y. Shen, I. Kaminer, H. Chen, and M. Soljačić, "Transverse-electric Brewster effect enabled by nonmagnetic two-dimensional materials," Phys. Rev. A **94**, 023836 (2016).
[93]J. Luo, H. Chu, R. Peng, M. Wang, J. Li, and Y. Lai, "Ultra-broadband reflectionless Brewster absorber protected by reciprocity," Light: Sci. Appl. **10**, 89 (2021).
[94]R. Chen, J. Chen, Z. Gong, X. Zhang, X. Zhu, Y. Yang, I. Kaminer, H. Chen, B. Zhang, and X. Lin, "Free-electron Brewster-transition radiation," Sci. Adv. **9**, eadh8098 (2023).
[95]Y. Shen, D. Ye, I. Celanovic, S. G. Johnson, J. D. Joannopoulos, and M. Soljačić, "Optical broadband angular selectivity," Science **343**, 1499–1501 (2014).
[96]Y. Shen, C. W. Hsu, Y. X. Yeng, J. D. Joannopoulos, and M. Soljačić, "Broadband angular selectivity of light at the nanoscale: Progress, applications, and outlook," Appl. Phys. Rev. **3**, 011103 (2016).
[97]E. D. Palik, *Handbook of Optical Constants of Solids* (Academic Press, 1998).
[98]V. L. Ginzburg, *Transition Radiation and Transition Scattering* (A. Hilger, 1990).
[99]R. Chen, Z. Gong, J. Chen, X. Zhang, X. Zhu, H. Chen, and X. Lin, "Recent advances of transition radiation: Fundamentals and applications," Mater. Today Electron. **3**, 100025 (2023).
[100]V. L. Gizburg and V. Tsytovich, "Several problems of the theory of transition radiation and transition scattering," Phys. Rep. **49**, 1–89 (1979).
[101]L. V. Rodríguez-de Marcos, J. I. Larruquert, J. A. Méndez, and J. A. Aznárez, "Self-consistent optical constants of SiO_2 and Ta_2O_5 films," Opt. Mater. Express **6**, 3622–3637 (2016).

[102]L. V. Rodríguez-de Marcos, J. I. Larruquert, J. A. Méndez, and J. A. Aznárez, "Self-consistent optical constants of MgF_2, LaF_3, and CeF_3 films," Opt. Mater. Express **7**, 989–1006 (2017).
[103]T. Cai, Y. Zhong, D. Liu, H. Huang, D. Wang, Y. Yang, H. Chen, and X. Lin, "Observation of polarization-maintaining near-field directionality," Prog. Electromagn. Res. **181**, 35–41 (2024).
[104]X. Zhang, J. Chen, R. Chen, C. Wang, T. Cai, R. Abdi-Ghaleh, H. Chen, and X. Lin, "Perspective on meta-boundaries," ACS Photonics **10**, 2102–2115 (2023).
[105]C. Wang, X. Chen, Z. Gong, R. Chen, H. Hu, H. Wang, Y. Yang, L. Tony, B. Zhang, and H. Chen, "Superscattering of light: Fundamentals and applications," Rep. Prog. Phys. **87**, 126401 (2024).

Supplementary information for

Achromatic interfacial Cherenkov radiation from photonic crystals

Xiangfeng Xi, Zheng Gong, Ruoxi Chen, Zun Wang, Owen D. Miller, Yi Yang, Hongsheng Chen, Ido Kaminer, and Xiao Lin

Supplementary Information Guide:

Section S1. Derivation of interfacial Cherenkov radiation from photonic crystals

In this section, we rigorously calculate the angular spectral energy density and field distribution of interfacial Cherenkov radiation by extending Ginzburg and Frank's theory of transition radiation from a single interface [100] to a multi-layer system with N interfaces and $N+1$ regions [7,29], as shown in Fig. S1.

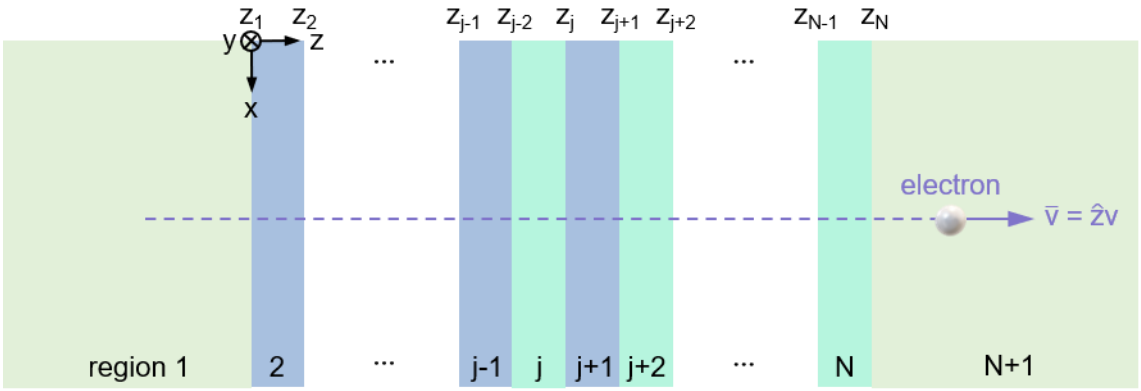

FIG. S1. Structural schematic of free-electron radiation from multiple parallel interfaces.

S1.1 Free-electron transition radiation from a single interface

In this subsection, we derive the transition radiation from a single optical interface. As shown in Fig. S1, when an electron with charge q and velocity $\hat{z}v$ perpendicularly penetrates the interface $z = z_j$ between region j and region $j+1$, transition radiation occurs in both the backward and forward directions. Accordingly, the induced current density from the moving electron is

$$\bar{J}^q(\bar{r},t) = \hat{z}qv\delta(x)\delta(y)\delta(z-vt) \tag{S1}$$

By performing Fourier transformation, equation (S1) can be expressed as

$$\bar{J}^q(\bar{r},t) = \hat{z}\int d\omega \int d\bar{k}_\perp J^q_{\bar{k}_\perp,\omega}(z)e^{i\bar{k}_\perp\bar{r}_\perp - i\omega t} \tag{S2}$$

where $\bar{k}_\perp = \hat{x}k_x + \hat{y}k_y$ is the wavevector component perpendicular to the electron velocity and $\bar{r}_\perp = \hat{x}x + \hat{y}y$. From equations (S1)-(S2), we have

$$J^{q}_{\bar{k}_{\perp},\omega}(z) = \frac{q}{(2\pi)^3} e^{i\omega z/v} \tag{S3}$$

Similarly, we apply the Fourier transformation to the electric field $\bar{E}(\bar{r},t)$ and the magnetic field $\bar{H}(\bar{r},t)$, namely

$$\bar{E}(\bar{r},t) = \hat{z}\int d\omega \int d\bar{k}_{\perp}\, \bar{E}_{\bar{k}_{\perp},\omega}(z) e^{i\bar{k}_{\perp}\bar{r}_{\perp} - i\omega t} \tag{S4}$$

$$\bar{H}(\bar{r},t) = \hat{z}\int d\omega \int d\bar{k}_{\perp}\, \bar{H}_{\bar{k}_{\perp},\omega}(z) e^{i\bar{k}_{\perp}\bar{r}_{\perp} - i\omega t} \tag{S5}$$

By solving Maxwell equations in $\bar{k}_{\perp}$ and ω space, the Helmholtz equations of $E_{\mathrm{z}}(z)$ and $H_{\mathrm{z}}(z)$ in the medium with permittivity ε and permeability μ can be written as

$$(\partial^2/\partial z^2 + \omega^2\mu\varepsilon - k_{\perp}^2)\begin{pmatrix} E_z \\ H_z \end{pmatrix} = \begin{pmatrix} -(\partial^2/\partial z^2 + \omega^2\mu\varepsilon)\dfrac{J_z}{i\omega\varepsilon} \\ 0 \end{pmatrix} \tag{S6}$$

Since $J_{\perp} = 0$, we have $H_z = 0$, meaning that all excited fields are *p*-polarized waves. Then, the solution of the primary field [108] E_z can be expressed as

$$E_z = E_z^q + E_z^R \tag{S7}$$

$$E^{q}_{z,j} = -\frac{iq}{\omega\varepsilon_0(2\pi)^3} \frac{1 - \dfrac{c^2}{v^2\varepsilon_{\mathrm{r},j}}}{\varepsilon_{\mathrm{r},j} - \dfrac{c^2}{v^2} - \dfrac{k_{\perp}^2 c^2}{\omega^2}} e^{i\frac{\omega}{v}z} \tag{S8}$$

$$E^{q}_{z,j+1} = -\frac{iq}{\omega\varepsilon_0(2\pi)^3} \frac{1 - \dfrac{c^2}{v^2\varepsilon_{\mathrm{r},j+1}}}{\varepsilon_{\mathrm{r},j+1} - \dfrac{c^2}{v^2} - \dfrac{k_{\perp}^2 c^2}{\omega^2}} e^{i\frac{\omega}{v}z} \tag{S9}$$

$$E^{R}_{z,j} = \frac{iq}{\omega\varepsilon_0(2\pi)^3} a^{-}_{j|j+1} e^{-ik_{z,j}(z-z_j)} \tag{S10}$$

$$E^{R}_{z,j+1} = \frac{iq}{\omega\varepsilon_0(2\pi)^3} a^{+}_{j|j+1} e^{ik_{z,j+1}(z-z_j)} \tag{S11}$$

where $\varepsilon_{\mathrm{r},j}$ is the relative permittivity of region j, and $k_{z,j} = \sqrt{\frac{\omega^2}{c^2}\varepsilon_{\mathrm{r},j} - k_{\perp}^2}$ is the z-component wavevector in region j. E_z^q corresponds to the charge field carried by the electron, and E_z^R corresponds to the radiation field emitted from the interface. $a^{-}_{j|j+1}$ ($a^{+}_{j|j+1}$) represents the backward (forward) radiation

factor from the $j|j+1$ interface at $z=z_j$. By matching the boundary conditions, one can obtain the two radiation factors as

$$a_{j,j+1}^{-}=a_{j,j+1}^{-,0}e^{i\frac{\omega}{v}z_j} \tag{S12}$$

$$a_{j,j+1}^{+}=a_{j,j+1}^{+,0}e^{i\frac{\omega}{v}z_j} \tag{S13}$$

$$a_{j,j+1}^{-,0}=\frac{\frac{k_\perp^2c^2}{\omega^2}\cdot\frac{-v}{c}\cdot\varepsilon_{\mathrm{r},j+1}}{\varepsilon_{\mathrm{r},j}\frac{k_{z,j+1}}{\omega/c}+\varepsilon_{\mathrm{r},j+1}\frac{k_{z,j}}{\omega/c}}\cdot\left[\frac{1-\frac{v}{c}\cdot\frac{k_{z,j+1}}{\omega/c}}{\varepsilon_{\mathrm{r},j+1}\left(1-\frac{v^2}{c^2}\varepsilon_{\mathrm{r},j+1}+\frac{k_\perp^2v^2}{\omega^2}\right)}-\frac{1-\frac{v}{c}\cdot\frac{k_{z,j+1}}{\omega/c}\cdot\frac{\varepsilon_{\mathrm{r},j}}{\varepsilon_{\mathrm{r},j+1}}}{\varepsilon_{\mathrm{r},j}\left(1-\frac{v^2}{c^2}\varepsilon_{\mathrm{r},j}+\frac{k_\perp^2v^2}{\omega^2}\right)}\right] \tag{S14}$$

$$a_{j,j+1}^{+,0}=\frac{\frac{k_\perp^2c^2}{\omega^2}\cdot\frac{v}{c}\cdot\varepsilon_{\mathrm{r},j}}{\varepsilon_{\mathrm{r},j}\frac{k_{z,j+1}}{\omega/c}+\varepsilon_{\mathrm{r},j+1}\frac{k_{z,j}}{\omega/c}}\cdot\left[\frac{1+\frac{v}{c}\cdot\frac{k_{z,j}}{\omega/c}}{\varepsilon_{\mathrm{r},j}\left(1-\frac{v^2}{c^2}\varepsilon_{\mathrm{r},j}+\frac{k_\perp^2v^2}{\omega^2}\right)}-\frac{1+\frac{v}{c}\cdot\frac{k_{z,j}}{\omega/c}\cdot\frac{\varepsilon_{\mathrm{r},j+1}}{\varepsilon_{\mathrm{r},j}}}{\varepsilon_{\mathrm{r},j+1}\left(1-\frac{v^2}{c^2}\varepsilon_{\mathrm{r},\perp,j+1}+\frac{k_\perp^2v^2}{\omega^2}\right)}\right] \tag{S15}$$

where $a_{j,j+1}^{-,0}$ ($a_{j,j+1}^{+,0}$) is the factor of backward (forward) radiation from the $j|j+1$ interface when $z_j=0$. In all, we can obtain field distribution in the cylindrical coordinates (ρ,ϕ,z) as

$$\bar{E}_j(\bar{r},t)=\bar{E}_j^q(\bar{r},t)+\bar{E}_j^R(\bar{r},t) \tag{S16}$$

$$\begin{aligned}\bar{E}_j^q(\bar{r},t)=\hat{z}\int_{-\infty}^{+\infty}d\omega\frac{-q}{8\pi\omega\varepsilon_0\varepsilon_{\mathrm{r},j}}\left(\frac{\omega^2}{c^2}\varepsilon_{\mathrm{r},j}-\frac{\omega^2}{v^2}\right)H_0^{(1)}\left(\rho\sqrt{\frac{\omega^2}{c^2}\varepsilon_{\mathrm{r},j}-\frac{\omega^2}{v^2}}\right)e^{i\frac{\omega}{v}z-i\omega t}\\+\hat{\rho}\int_{-\infty}^{+\infty}d\omega\frac{iq}{8\pi v\varepsilon_0\varepsilon_{\mathrm{r},j}}\sqrt{\frac{\omega^2}{c^2}\varepsilon_{\mathrm{r},j}-\frac{\omega^2}{v^2}}H_1^{(1)}(\rho\sqrt{\frac{\omega^2}{c^2}\varepsilon_{\mathrm{r},j}-\frac{\omega^2}{v^2}})e^{i\frac{\omega}{v}z-i\omega t}\end{aligned} \tag{S17}$$

$$\begin{aligned}\bar{E}_j^R(\bar{r},t)=\hat{z}\int_{-\infty}^{+\infty}d\omega\int_0^{+\infty}dk_\perp\cdot\frac{iq}{\omega\varepsilon_0(2\pi)^3}a_{j|j+1}^{-}k_\perp2\pi J_0(k_\perp\rho)e^{-ik_{z,j}(z-z_j)-i\omega t}\\+\hat{\rho}\int_{-\infty}^{+\infty}d\omega\int_0^{+\infty}dk_\perp\cdot\frac{-q}{\omega\varepsilon_0(2\pi)^3}a_{j|j+1}^{-}k_{z,j}2\pi J_1(k_\perp\rho)e^{-ik_{z,j}(z-z_j)-i\omega t}\end{aligned} \tag{S18}$$

$$\begin{aligned}\bar{E}_{j+1}^q(\bar{r},t)=\hat{z}\int_{-\infty}^{+\infty}d\omega\frac{-q}{8\pi\omega\varepsilon_0\varepsilon_{\mathrm{r},j+1}}\left(\frac{\omega^2}{c^2}\varepsilon_{\mathrm{r},j+1}-\frac{\omega^2}{v^2}\right)H_0^{(1)}\left(\rho\sqrt{\frac{\omega^2}{c^2}\varepsilon_{\mathrm{r},j+1}-\frac{\omega^2}{v^2}}\right)e^{i\frac{\omega}{v}z-i\omega t}\\+\hat{\rho}\int_{-\infty}^{+\infty}d\omega\frac{iq}{8\pi v\varepsilon_0\varepsilon_{\mathrm{r},j+1}}\sqrt{\frac{\omega^2}{c^2}\varepsilon_{\mathrm{r},j+1}-\frac{\omega^2}{v^2}}H_1^{(1)}(\rho\sqrt{\frac{\omega^2}{c^2}\varepsilon_{\mathrm{r},j+1}-\frac{\omega^2}{v^2}})e^{i\frac{\omega}{v}z-i\omega t}\end{aligned} \tag{S19}$$

$$\begin{aligned}\bar{E}_{j+1}^R(\bar{r},t)=\hat{z}\int_{-\infty}^{+\infty}d\omega\int_0^{+\infty}dk_\perp\cdot\frac{iq}{\omega\varepsilon_0(2\pi)^3}a_{j|j+1}^{+}k_\perp2\pi J_0(k_\perp\rho)e^{ik_{z,j+1}(z-z_j)-i\omega t}\\+\hat{\rho}\int_{-\infty}^{+\infty}d\omega\int_0^{+\infty}dk_\perp\cdot\frac{q}{\omega\varepsilon_0(2\pi)^3}a_{j|j+1}^{+}k_{z,j+1}2\pi J_1(k_\perp\rho)e^{ik_{z,j+1}(z-z_j)-i\omega t}\end{aligned} \tag{S20}$$

where J_0 and J_1 represent the first kind of Bessel function of zero order and first order; $H_0^{(1)}$ and $H_1^{(1)}$

represent the first kind of Hankel function of zero order and first order, respectively.

S1.2 Interference of transition radiation from multiple parallel interfaces

In this subsection, we rigorously calculated the interference of transition radiation from multiple parallel interfaces. As schematically shown in Fig. S1, the total electromagnetic field in region j originates from both the interfaces above region j and those below it. First, we analyze the parts 1, 2 and 3 of the radiation contributed by the light emission at the interfaces above region j; subsequently, the field in region j resulted from the transition radiation at the interfaces below region j is derived in parts 4, 5 and 6.

Part 1: Field distribution in region j from the forward transition radiation at the $z = z_{j-1}$ interface

From the viewpoint of geometric optics, the forward transition radiation at the $z = z_{j-1}$ interface contributing to the field in region j is

$$TR^{+}_{(j-1)\to j} = F^{+}_{(j-1)\to j} \cdot \left[e^{ik_{z,j}(z-z_{j-1})} + \tilde{R}_{j|j+1} e^{2ik_{z,j}(z_j-z_{j-1})} e^{-ik_{z,j}(z-z_{j-1})}\right]$$
$$F^{+}_{(j-1)\to j} = \frac{iq}{\omega\varepsilon_0(2\pi)^3} \cdot a^{+}_{j-1|j} \cdot M_j$$
$$M_j = \frac{1}{1 - \tilde{R}_{j|j+1}\tilde{R}_{j|j-1} e^{2ik_{z,j}(z_j-z_{j-1})}} \tag{S21}$$

where the factor M_j characterizes the multiple reflections in region j at the $j|j-1$ and $j|j+1$ interfaces; $\tilde{R}_{j|j-1}$ and $\tilde{R}_{j|j+1}$ are the generalized reflection and transmission coefficients for *p*-polarized waves at the $j|j-1$ and $j|j+1$ interfaces, respectively. The subscript of $\tilde{R}_{j|j-1}$ and $\tilde{R}_{j|j+1}$ represents that *p*-polarized wave is incident from region j (the first number) and transmitted to region $j+1$ or $j-1$ (the second number), respectively. $\tilde{R}_{j|j-1}$ and $\tilde{R}_{j|j+1}$ can be obtained by

$$\tilde{R}_{j|j-1} = R_{j|j-1} + \frac{T_{j|j-1}\tilde{R}_{j-1|j-2}T_{j-1|j} e^{2ik_{z,j-1}(z_{j-1}-z_{j-2})}}{1 - R_{j-1|j}\tilde{R}_{j-1|j-2} e^{2ik_{z,j-1}(z_{j-1}-z_{j-2})}}$$
$$\tilde{R}_{j|j+1} = R_{j|j+1} + \frac{T_{j|j+1}\tilde{R}_{j+1|j+2}T_{j+1|j} e^{2ik_{z,j+1}(z_{j+1}-z_j)}}{1 - R_{j+1|j}\tilde{R}_{j+1|j+2} e^{2ik_{z,j+1}(z_{j+1}-z_j)}} \tag{S22}$$

These iteration relationships have the initial value $\tilde{R}_{2|1} = R_{2|1}$ and $\tilde{R}_{N|N+1} = R_{N|N+1}$. The reflection and transmission coefficients defined for E_z from region j to region $j+1$ can be expressed as $R_{j|j+1} = \frac{\varepsilon_{r,j+1}k_{z,j} - \varepsilon_{r,j}k_{z,j+1}}{\varepsilon_{r,j+1}k_{z,j} + \varepsilon_{r,j}k_{z,j+1}}$ and $T_{j|j+1} = \frac{2\varepsilon_{r,j}k_{z,j}}{\varepsilon_{r,j+1}k_{z,j} + \varepsilon_{r,j}k_{z,j+1}}$.

Part 2: Field distribution in region j from the forward transition radiation at the $z = z_m$ $(1 \le m \le j-2)$ interface

Firstly, the field distribution in region $m+1$ from the forward transition radiation at the $z = z_m$ interface can be obtained from equation (S21) as

$$TR^{+}_{m\to m+1} = F^{+}_{m\to m+1} \cdot \left[e^{ik_{z,m+1}(z-z_m)} + \tilde{R}_{m+1|m+2} e^{2ik_{z,m+1}(z_{m+1}-z_m)} e^{-ik_{z,m+1}(z-z_m)}\right]$$
$$F^{+}_{m\to m+1} = \frac{iq}{\omega\varepsilon_0(2\pi)^3} \cdot a^{+}_{m|m+1} \cdot M_{m+1} \tag{S23}$$

Then, from the viewpoint of geometric optics, the generalized forward radiation factor $F^{+}_{m\to m+2}$ in region $m+2$ originating from the forward transition radiation at the $z = z_m$ interface can be obtained as

$$F^{+}_{m\to m+2} \cdot e^{ik_{z,m+2}(z_{m+1}-z_m)} = F^{+}_{m\to m+1} \cdot S_{m+1|m+2} e^{ik_{z,m+1}(z_{m+1}-z_m)}$$
$$S_{m|m+1} = \frac{T_{m|m+1}}{1 - R_{m+1|m}\tilde{R}_{m+1|m+2} e^{2ik_{z,m+1}(z_{m+1}-z_m)}} \tag{S24}$$

Thus, $F^{+}_{m\to m+2}$ can be derived analytically from $F^{+}_{m\to m+1}$. From this iteration relationship, the generalized forward radiation factor $F^{+}_{m\to j}$ in region j originating from the forward transition radiation at the $z = z_m$ interface can be expressed as

$$F^{+}_{m\to j} \cdot e^{ik_{z,j}(z_{j-1}-z_m)} = F^{+}_{m\to m+1} \cdot \prod_{n=m+1}^{j-1} S_{n|n+1}\, e^{ik_{z,n}(z_n - z_{n-1})} \tag{S25}$$

As a result, the forward transition radiation at the $z = z_m$ interface contributing to the field in region j is

$$TR^{+}_{m\to j} = F^{+}_{m\to j} \cdot \left[e^{ik_{z,j}(z-z_m)} + \tilde{R}_{j|j+1} e^{2ik_{z,j}(z_j-z_m)} e^{-ik_{z,j}(z-z_m)}\right] \tag{S26}$$

Part 3: Field distribution in region j from the forward transition radiation at the $z = z_m$ $(j \le m \le N)$ interface

Firstly, the generalized backward radiation factor $F^{-}_{m\to m+1}$ in region $m+1$ originating from the forward transition radiation at the $z = z_m$ interface can be obtained from equation (S21) as

$$F_{m\to m+1}^{-} = F_{m\to m+1}^{+}\tilde{R}_{m+1|m+2}e^{2ik_{z,m+1}(z_{m+1}-z_m)} \tag{S27}$$

Then, from the viewpoint of geometric optics, the generalized backward radiation factor $F_{m\to m}^{-}$ in region m originating from the forward transition radiation at the $z = z_m$ interface can be obtained as

$$F_{m\to m}^{-}\cdot e^{-ik_{z,m}(z_m-z_m)} = F_{m\to m+1}^{+}\cdot e^{-ik_{z,m+1}(z_{m+1}-z_m)}S_{m+1|m}e^{-ik_{z,m+1}(z_m-z_{m+1})}$$
$$S_{m+1|m} = \frac{T_{m+1|m}}{1-R_{m|m+1}\tilde{R}_{m|m-1}e^{2ik_{z,m}(z_m-z_{m-1})}} \tag{S28}$$

Thus, $F_{m\to m}^{-}$ can be derived analytically from $F_{m\to m+1}^{-}$. From this iteration relationship, the generalized forward radiation factor $F_{m\to j}^{-}$ in region j originating from the forward transition radiation at the $z = z_m$ interface can be expressed as

$$F_{m\to j}^{-}\cdot e^{-ik_{z,j}(z_j-z_m)} = F_{m\to m+1}^{-}\cdot e^{-ik_{z,m+1}(z_{m+1}-z_m)}\cdot\prod_{n=j}^{m}S_{n+1|n}\,e^{-ik_{z,n+1}(z_n-z_{n+1})} \tag{S29}$$

As a result, the forward transition radiation at the $z = z_m$ interface contributing to the field in region j is

$$TR_{m\to j}^{-} = F_{m\to j}^{-}\cdot\left[e^{-ik_{z,j}(z-z_m)} + \tilde{R}_{j|j-1}e^{-2ik_{z,j}(z_{j-1}-z_m)}e^{ik_{z,j}(z-z_m)}\right] \tag{S30}$$

Part 4: Field distribution in region j from the backward transition radiation at the $z = z_j$ interface

From the viewpoint of geometric optics, the backward transition radiation at the $z = z_j$ interface contributing to the field in region j is

$$TR_{j\to j}^{-} = B_{j\to j}^{-}\cdot\left[e^{-ik_{z,j}(z-z_j)} + \tilde{R}_{j|j-1}e^{-2ik_{z,j}(z_{j-1}-z_j)}e^{ik_{z,j}(z-z_j)}\right]$$
$$B_{j\to j}^{-} = \frac{iq}{\omega\varepsilon_0(2\pi)^3}\cdot a_{j|j+1}^{-}\cdot M_j \tag{S31}$$

Part 5: Field distribution in region j from the backward transition radiation at the $z = z_m$ $(j+1 \le m \le N)$ interface

Firstly, the field distribution in region m from the backward transition radiation at the $z = z_m$ interface can be obtained from equation (S31) as

$$TR_{m\to m+1}^{-} = B_{m\to m}^{-}\cdot\left[e^{-ik_{z,m}(z-z_m)} + \tilde{R}_{m|m-1}e^{-2ik_{z,m}(z_{m-1}-z_m)}e^{ik_{z,m}(z-z_m)}\right] \tag{S32}$$

Then, from the viewpoint of geometric optics, the generalized backward radiation factor $B_{m\to m-1}^{-}$ in region $m-1$ originating from the backward transition radiation at the $z = z_m$ interface can be obtained as

$$B_{m\to m-1}^{-}\cdot e^{-ik_{z,m-1}(z_{m-1}-z_m)}=B_{m\to m}^{-}\cdot S_{m|m-1}e^{-ik_{z,m}(z_{m-1}-z_m)} \tag{S33}$$

Thus, $B_{m\to m-1}^{-}$ can be derived analytically from $B_{m\to m}^{-}$. From this iteration relationship, the generalized forward radiation factor $B_{m\to j}^{-}$ in region j originating from the backward transition radiation at the $z=z_m$ interface can be expressed as

$$B_{m\to j}^{-}\cdot e^{-ik_{z,j}(z_j-z_m)}=B_{m\to m}^{-}\cdot\prod_{n=j}^{m-1}S_{n+1|n}\,e^{-ik_{z,n+1}(z_n-z_{n+1})} \tag{S34}$$

As a result, the backward transition radiation at the $z=z_m$ interface contributing to the field in region j is

$$TR_{m\to j}^{-}=B_{m\to j}^{-}\cdot\left[e^{-ik_{z,j}(z-z_m)}+\tilde{R}_{j|j-1}e^{-2ik_{z,j}(z_{j-1}-z_m)}e^{ik_{z,j}(z-z_m)}\right] \tag{S35}$$

Part 6: Field distribution in region j from the backward transition radiation at the $z=z_m$ $(1\le m\le j-1)$ interface

Firstly, the generalized forward radiation factor $B_{m\to m}^{+}$ in region m originating from the backward transition radiation at the $z=z_m$ interface can be obtained from equation (S31) as

$$B_{m\to m}^{+}=B_{m\to m}^{-}\tilde{R}_{m|m-1}e^{-2ik_{z,m}(z_{m-1}-z_m)} \tag{S36}$$

Then, from the viewpoint of geometric optics, the generalized forward radiation factor $B_{m\to m+1}^{+}$ in region $m+1$ originating from the backward transition radiation at the $z=z_m$ interface can be obtained as

$$B_{m\to m+1}^{+}\cdot e^{ik_{z,m+1}(z_m-z_m)}=B_{m\to m}^{+}\cdot e^{ik_{z,m}(z_{m-1}-z_m)}S_{m|m+1}e^{ik_{z,m}(z_m-z_{m-1})} \tag{S37}$$

Thus, $B_{m\to m+1}^{+}$ can be derived analytically from $B_{m\to m}^{+}$. From this iteration relationship, the generalized forward radiation factor $B_{m\to j}^{+}$ in region j originating from the backward transition radiation at the $z=z_m$ interface can be expressed as

$$B_{m\to j}^{+}\cdot e^{ik_{z,j}(z_{j-1}-z_m)}=B_{m\to m}^{+}\cdot e^{ik_{z,m}(z_{m-1}-z_m)}\cdot\prod_{n=m}^{j-1}S_{n|n+1}\,e^{ik_{z,n}(z_n-z_{n-1})} \tag{S38}$$

Thus, the field in region j contributed by backward transition radiation at the $z=z_m$ interface is

$$TR_{m\to j}^{+} = B_{m\to j}^{+} \cdot \left[e^{ik_{z,j}(z-z_m)} + \tilde{R}_{j|j+1} e^{2ik_{z,j}(z_j-z_m)} e^{-ik_{z,j}(z-z_m)}\right] \tag{S39}$$

Part 7: Interference of transition radiation from multiple parallel interfaces

From above analysis, the total electric field in each region j $(1 \le j \le N+1)$ can be expressed as

$$E_{z,j}^{R} = \begin{cases} \dfrac{iq}{\omega\varepsilon_0(2\pi)^3} a_1 e^{-ik_{z,1}(z-z_1)} & (j=1) \\ \dfrac{iq}{\omega\varepsilon_0(2\pi)^3}\left[a_j^{+} e^{ik_{z,j}(z-z_{j-1})} + a_j^{-} e^{-ik_{z,j}(z-z_j)}\right] & (2 \le j \le N-1) \\ \dfrac{iq}{\omega\varepsilon_0(2\pi)^3} a_{N+1} e^{-ik_{z,N+1}(z-z_N)} & (j=N+1) \end{cases} \tag{S40}$$

where a_j^{+} (a_j^{-}) represents the generalized forward (backward) radiation factor in region j, and can be derived by parts 1-6. For regions $j=1$ and $j=N+1$, the radiation propagates along the $-z$ and $+z$ directions, respectively. For $j=1$, the generalized backward radiation factor a_1 can be expressed as

$$a_1 = \frac{\omega\varepsilon_0(2\pi)^3}{iq} \cdot \left[\sum_{m=1}^{N} (F_{m\to 1}^{-} + B_{m\to 1}^{-}) e^{ik_{z,1}(z_m-z_1)}\right] \tag{S41}$$

For $j=N+1$, the generalized forward radiation factor a_{N+1} can be expressed as

$$a_{N+1} = \frac{\omega\varepsilon_0(2\pi)^3}{iq} \cdot \left[\sum_{m=1}^{N} (F_{m\to N+1}^{+} + B_{m\to N+1}^{+}) e^{-ik_{z,1}(z_m-z_N)}\right] \tag{S42}$$

S1.3 Angular spectral energy density of interfacial Cherenkov radiation

In this subsection we calculate the forward angular spectral energy density $U(\theta_{\text{out}}, \lambda)$ of the interfacial Cherenkov radiation. $U(\theta_{\text{out}}, \lambda)$ can be expressed as

$$W = \int_0^{+\infty} d\omega \int_0^{\pi/2} d\theta_{\text{out}}\, U(\theta_{\text{out}}, \lambda) \cdot 2\pi \sin(\theta_{\text{out}}) \tag{S43}$$

where θ_{out} is the angle between the wavevector $\bar{k}_{\text{out}}$ of light in region $N+1$ and the electron velocity $\bar{v}$, and W is total energy of the forward radiation field in region $N+1$. For a long time t, the radiation field E^R is already at a great distance to the interface and separated from the charge field E^q and the electric and magnetic energy densities are equal in superstrate. This way, W can be obtained by integrating the radiation field energy density across all space as

$$W = \iint dxdy \int_{-\infty}^{+\infty} dz\, \varepsilon_{N+1} |\bar{E}_{N+1}^{R}(\bar{r}, \mathrm{t})|^2 \tag{S44}$$

$$|\bar{E}_{N+1}^{R}(\bar{r}, \mathrm{t})|^2 = \int d\omega d\omega' \iint d\bar{k}_{\perp} d\bar{k}'_{\perp}\, \bar{E}_{\bar{k}_{\perp},\omega,N+1}^{R}(z) \cdot \left[\bar{E}_{\bar{k}'_{\perp},\omega',N+1}^{R}(z)\right]^{*} e^{i[(\bar{k}_{\perp}-\bar{k}'_{\perp})\cdot\bar{r}_{\perp}-(\omega-\omega')t]} \tag{S45}$$

By substituting equation (S45) into equation (S44), and integrating over $dxdyd\bar{k}'_{\perp}dzd\omega'$, we have

$$W = 2\int_{0}^{+\infty} d\omega \int \varepsilon_{N+1} |a_{N+1}|^2 \left(\frac{q}{\omega\varepsilon_0(2\pi)^3}\right)^2 \frac{\omega^2\sqrt{\varepsilon_{\mathrm{r,N+1}}}}{ck_{\perp}^2} \sqrt{1-\frac{c^2k_{\perp}^2}{\omega^2\varepsilon_{\mathrm{r},N+1}}}\,(2\pi)^3 d\bar{k}_{\perp} \tag{S46}$$

For emitted photons, the integration over $d\bar{k}_{\perp}$ should be taken over the range $k_{\perp}^2 \le \frac{\omega^2}{c^2}\varepsilon_{\mathrm{r},N+1}$. Then, by comparing equation (S43), the forward angular spectral energy density of interfacial Cherenkov radiation can be expressed as

$$U(\theta_{\mathrm{out}}, \lambda) = |a_{N+1}|^2 \cdot \frac{\varepsilon_{\mathrm{r},N+1}^{3/2} q^2 \cos^2(\theta_{\mathrm{out}})}{4\pi^3\varepsilon_0 c \sin^2(\theta_{\mathrm{out}})} \tag{S47}$$

S1.4 Field distribution of excited interfacial Cherenkov radiation

By following the same procedure as equations (S16)-(S20), the field distribution can be written as

$$\bar{E}_j(\bar{r}, t) = \bar{E}_j^{q}(\bar{r}, t) + \bar{E}_j^{R}(\bar{r}, t) \tag{S48}$$

$$\begin{aligned}\bar{E}_j^{q}(\bar{r}, t) = \hat{z}\int_{-\infty}^{+\infty} d\omega \frac{-q}{8\pi\omega\varepsilon_0\varepsilon_{\mathrm{r},j}}\left(\frac{\omega^2}{c^2}\varepsilon_{\mathrm{r},j} - \frac{\omega^2}{v^2}\right) H_0^{(1)}\left(\rho\sqrt{\frac{\omega^2}{c^2}\varepsilon_{\mathrm{r},j} - \frac{\omega^2}{v^2}}\right) e^{i\frac{\omega}{v}z - i\omega t} \\ +\hat{\rho}\int_{-\infty}^{+\infty} d\omega \frac{iq}{8\pi v\varepsilon_0\varepsilon_{\mathrm{r},j}}\sqrt{\frac{\omega^2}{c^2}\varepsilon_{\mathrm{r},j} - \frac{\omega^2}{v^2}}\, H_1^{(1)}(\rho\sqrt{\frac{\omega^2}{c^2}\varepsilon_{\mathrm{r},j} - \frac{\omega^2}{v^2}}) e^{i\frac{\omega}{v}z - i\omega t}\end{aligned} \tag{S49}$$

$$\begin{aligned}\bar{E}_j^{R}(\bar{r}, t) = \hat{z}\int d\omega\, dk_{\perp} \frac{iq}{\omega\varepsilon_0(2\pi)^3} k_{\perp} 2\pi J_0(k_{\perp}\rho)\left[a_j^{-} e^{-ik_{z,j}(z-z_j)-i\omega t} + a_j^{+} e^{ik_{z,j}(z-z_{j-1})-i\omega t}\right] \\ +\hat{\rho}\int d\omega\, dk_{\perp} \frac{-q}{\omega\varepsilon_0(2\pi)^3} k_{z,j} 2\pi J_1(k_{\perp}\rho)\left[a_j^{-} e^{-ik_{z,j}(z-z_j)-i\omega t} + a_j^{+} e^{ik_{z,j}(z-z_{j-1})-i\omega t}\right]\end{aligned} \tag{S50}$$

where the generalized forward (backward) radiation factor in region j, namely a_j^{+} (a_j^{-}), and can be derived by parts 1-7 of the section S1.3.

Section S2. Derivation of conventional bulk Cherenkov radiation from the effective homogeneous achromatic uniaxial slab.

In this section, we derive the conventional bulk Cherenkov radiation from a finite-thickness uniaxial slab. To this end, we generally consider the free-electron radiation (including Cherenkov radiation and transition radiation) from a uniaxial slab, as illustrated in Fig. S2.

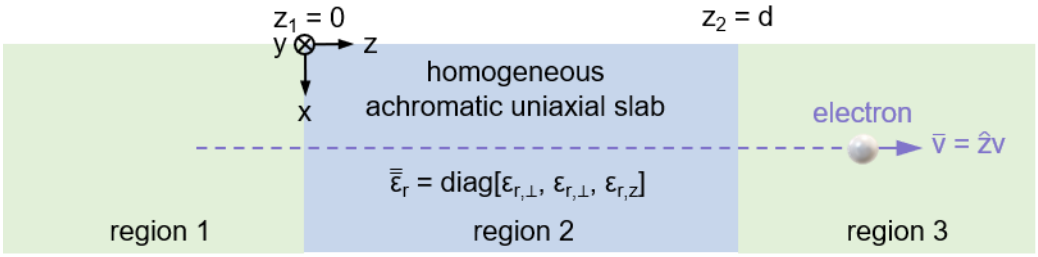

FIG. S2. Free-electron radiation from a uniaxial slab.

The derivation follows an analogous methodology to Section S1, while considering an anisotropic permittivity tensor $\bar{\bar{\varepsilon}}_{\mathrm{r},j} = \mathrm{diag}\left[\varepsilon_{\mathrm{r},\perp,j}, \varepsilon_{\mathrm{r},\perp,j}, \varepsilon_{\mathrm{r},z,j}\right]$. For single-interface transition radiation under uniaxial media conditions, the general field expressions in equations (S10)-(S13) remain unchanged, while the radiation factors $a_{j,j+1}^{-,0}$ and $a_{j,j+1}^{+,0}$ are modified as

$$a_{j,j+1}^{-,0} = \frac{\frac{k_\perp^2 c^2}{\omega^2}\cdot\frac{-v}{c}\cdot\frac{\varepsilon_{\mathrm{r},\perp,j}\varepsilon_{\mathrm{r},\perp,j+1}}{\varepsilon_{\mathrm{r},z,j}}}{\varepsilon_{\mathrm{r},\perp,j}\frac{k_{z,j+1}}{\omega/c}+\varepsilon_{\mathrm{r},\perp,j+1}\frac{k_{z,j}}{\omega/c}}\cdot\left[\frac{1-\frac{v}{c}\cdot\frac{k_{z,j+1}}{\omega/c}}{\varepsilon_{\mathrm{r},z,j+1}\left(1-\frac{v^2}{c^2}\varepsilon_{\mathrm{r},\perp,j+1}+\frac{k_\perp^2 v^2}{\omega^2}\frac{\varepsilon_{\mathrm{r},\perp,j+1}}{\varepsilon_{\mathrm{r},z,j+1}}\right)}-\frac{1-\frac{v}{c}\cdot\frac{k_{z,j+1}}{\omega/c}\cdot\frac{\varepsilon_{\mathrm{r},\perp,j}}{\varepsilon_{\mathrm{r},\perp,j+1}}}{\varepsilon_{\mathrm{r},z,j}\left(1-\frac{v^2}{c^2}\varepsilon_{\mathrm{r},\perp,j}+\frac{k_\perp^2 v^2}{\omega^2}\frac{\varepsilon_{\mathrm{r},\perp,j}}{\varepsilon_{\mathrm{r},z,j}}\right)}\right] \tag{S51}$$

$$a_{j,j+1}^{+,0} = \frac{\frac{k_\perp^2 c^2}{\omega^2}\cdot\frac{v}{c}\cdot\frac{\varepsilon_{\mathrm{r},\perp,j}\varepsilon_{\mathrm{r},\perp,j+1}}{\varepsilon_{\mathrm{r},z,j+1}}}{\varepsilon_{\mathrm{r},\perp,j}\frac{k_{z,j+1}}{\omega/c}+\varepsilon_{\mathrm{r},\perp,j+1}\frac{k_{z,j}}{\omega/c}}\cdot\left[\frac{1+\frac{v}{c}\cdot\frac{k_{z,j}}{\omega/c}}{\varepsilon_{\mathrm{r},z,j}\left(1-\frac{v^2}{c^2}\varepsilon_{\mathrm{r},\perp,j}+\frac{k_\perp^2 v^2}{\omega^2}\frac{\varepsilon_{\mathrm{r},\perp,j}}{\varepsilon_{\mathrm{r},z,j}}\right)}-\frac{1+\frac{v}{c}\cdot\frac{k_{z,j}}{\omega/c}\cdot\frac{\varepsilon_{\mathrm{r},\perp,j+1}}{\varepsilon_{\mathrm{r},\perp,j}}}{\varepsilon_{\mathrm{r},z,j+1}\left(1-\frac{v^2}{c^2}\varepsilon_{\mathrm{r},\perp,j+1}+\frac{k_\perp^2 v^2}{\omega^2}\frac{\varepsilon_{\mathrm{r},\perp,j+1}}{\varepsilon_{\mathrm{r},z,j+1}}\right)}\right] \tag{S52}$$

where $k_{z,j} = \sqrt{\frac{\varepsilon_{r,\perp,j}\omega^2}{c^2} - k_\perp^2\frac{\varepsilon_{r,\perp,j}}{\varepsilon_{r,z,j}}}$. The field distribution in each region can still be expressed by equation (S40). Specifically, the generalized radiation factor in each region can be obtained as

$$a_1^- = a_{1,2}^{-,0} + a_{1,2}^{+,0}\frac{T_{21}R_{23}e^{2ik_{\mathrm{z},2}d}}{1-R_{21}R_{23}e^{2ik_{\mathrm{z},2}d}} + a_{2,3}^{-,0}\frac{T_{21}e^{ik_{\mathrm{z},2}d+i\frac{\omega}{v}d}}{1-R_{21}R_{23}e^{2ik_{\mathrm{z},2}d}} \tag{S53}$$

$$a_2^- = a_{1,2}^{+,0}\frac{R_{23}e^{i2k_{\mathrm{z},2}d}}{1-R_{21}R_{23}e^{2ik_{\mathrm{z},2}d}} + a_{2,3}^{-,0}\frac{e^{ik_{\mathrm{z},2}d+i\frac{\omega}{v}d}}{1-R_{21}R_{23}e^{2ik_{\mathrm{z},2}d}} \tag{S54}$$

$$a_2^+ = a_{1,2}^{+,0}\frac{1}{1-R_{21}R_{23}e^{2ik_{z,2}d}} + a_{2,3}^{-,0}\frac{R_{21}e^{i2k_{z,2}d+i\frac{\omega}{v}d}}{1-R_{21}R_{23}e^{2ik_{z,2}d}} \tag{S55}$$

$$a_3^+ = a_{2,3}^{+,0}e^{i\frac{\omega}{v}d} + a_{1,2}^{+,0}\frac{T_{23}e^{ik_{z,2}d}}{1-R_{21}R_{23}e^{2ik_{z,2}d}} + a_{2,3}^{-,0}\frac{T_{23}R_{21}e^{2ik_{z,2}d}e^{i\frac{\omega}{v}d}}{1-R_{21}R_{23}e^{2ik_{z,2}d}} \tag{S56}$$

where the reflection and transmission coefficients are changed to $R_{j|j+1} = \frac{\varepsilon_{\mathrm{r},\perp,j+1}k_{z,j} - \varepsilon_{\mathrm{r},\perp,j}k_{z,j+1}}{\varepsilon_{\mathrm{r},\perp,j+1}k_{z,j} + \varepsilon_{\mathrm{r},\perp,j}k_{z,j+1}}$ and $T_{j|j+1} = \frac{2\varepsilon_{\mathrm{r},\perp,j+1}k_{z,j}}{\varepsilon_{\mathrm{r},\perp,j+1}k_{z,j} + \varepsilon_{\mathrm{r},\perp,j}k_{z,j+1}} \cdot \frac{\varepsilon_{\mathrm{r},z,j}}{\varepsilon_{\mathrm{r},z,j+1}}$, respectively. The forward angular spectral energy densities of transition radiation from a uniaxial slab can still be expressed by equation (S47), namely

$$U(\theta_{\mathrm{out}},\lambda) = |a_3^+|^2 \cdot \frac{\varepsilon_{\mathrm{r},3}^{3/2}q^2\cos^2(\theta_{\mathrm{out}})}{4\pi^3\varepsilon_0 c\sin^2(\theta_{\mathrm{out}})} \tag{S57}$$

Section S3. More discussion on achromatic interfacial Cherenkov radiation from photonic crystals

S3.1 Derivation of anomalous Maxwell-Garnett theory via Brewster effect for achromatic interfacial Cherenkov radiation

In this subsection, we derive the anomalous Maxwell-Garnett theory via Brewster effect for interfacial Cherenkov radiation. The dispersion for *p*-polarized light inside the photonic crystal is derived as

$$\cos(k_z d) = \left[\cos(k_{z,1}d_1)\cos(k_{z,2}d_2) - \frac{1}{2}\left(\frac{\tilde{\eta}_1}{\tilde{\eta}_2} + \frac{\tilde{\eta}_2}{\tilde{\eta}_1}\right)\sin(k_{z,1}d_1)\sin(k_{z,2}d_2)\right] \tag{S58}$$

where $\tilde{\eta}_X = \frac{k_{z,X}}{\omega\varepsilon_0\varepsilon_{\mathrm{r},X}}$, and X is either 1 or 2. When the impedance-matching condition $\tilde{\eta}_1 = \tilde{\eta}_2$ is fulfilled, namely

$$\frac{k_{z,1}}{\varepsilon_{\mathrm{r},1}} - \frac{k_{z,2}}{\varepsilon_{\mathrm{r},2}} = 0 \tag{S59}$$

we have $\frac{1}{2}\left(\frac{\tilde{\eta}_1}{\tilde{\eta}_2} + \frac{\tilde{\eta}_2}{\tilde{\eta}_1}\right) = 1$, and equation (S58) can be reduced to $\cos(k_{z,\mathrm{B}}d) = \cos(k_{z,1}d_1)\cos(k_{z,2}d_2) - \sin(k_{z,1}d_1)\sin(k_{z,2}d_2)$, namely $\cos(k_{z,\mathrm{B}}d) = \cos(k_{z,1}d_1 + k_{z,2}d_2)$. As a result, under the impedance-matching condition, one simple solution to equation (S58) is

$$k_{z,\mathrm{B}}d = k_{z,1}d_1 + k_{z,2}d_2 \tag{S60}$$

Square both sides of equation (S60), we obtain

$$k_{z,\mathrm{B}}^2 d^2 = k_{z,1}^2 d_1^2 + k_{z,2}^2 d_2^2 + 2k_{z,1}d_1k_{z,2}d_2 \tag{S61}$$

By further squaring both sides of equation (S59), one has

$$2k_{z,1}k_{z,2} = \frac{\varepsilon_{\mathrm{r},1}^2 k_{z,1}^2 + \varepsilon_{\mathrm{r},2}^2 k_{z,2}^2}{\varepsilon_{\mathrm{r},1}\varepsilon_{\mathrm{r},2}} \tag{S62}$$

Substituting equation (S62) into equation (S61) yields

$$k_{z,\mathrm{B}}^2 d^2 = k_{z,1}^2 d_1^2 + k_{z,2}^2 d_2^2 + \left(\frac{\varepsilon_{\mathrm{r},1}^2 k_{z,1}^2 + \varepsilon_{\mathrm{r},2}^2 k_{z,2}^2}{\varepsilon_{\mathrm{r},1}\varepsilon_{\mathrm{r},2}}\right) d_1 d_2 \tag{S63}$$

The $k_{z,X}$ and $k_{\perp,\mathrm{B}}$ is connected by the dispersion of the dielectric, i.e. $k_{z,X}^2 + k_{\perp,\mathrm{B}}^2 = \varepsilon_{\mathrm{r},X}\frac{\omega^2}{c^2}$. We substitute $k_{z,X}^2 = \varepsilon_{\mathrm{r},X}\frac{\omega^2}{c^2} - k_{\perp,\mathrm{B}}^2$ into equation (S63), and after some calculations, we arrive at

$$\frac{k_{\perp,\mathrm{B}}^2}{\frac{\varepsilon_{\mathrm{r},1}\varepsilon_{\mathrm{r},2}(d_1+d_2)}{\varepsilon_{\mathrm{r},1}d_2 + \varepsilon_{\mathrm{r},2}d_1}} + \frac{k_{z,\mathrm{B}}^2}{\frac{\varepsilon_{\mathrm{r},1}d_1 + \varepsilon_{\mathrm{r},2}d_2}{d_1+d_2}} = \frac{\omega^2}{c^2} \tag{S64}$$

By comparing equation (S64) with the standard dispersion relation of uniaxial medium, namely $\frac{k_\perp^2}{\varepsilon_{\mathrm{eff},z}} + \frac{k_z^2}{\varepsilon_{\mathrm{eff},\perp}} = \frac{\omega^2}{c^2}$, one has $\varepsilon_{\mathrm{eff},\perp} = \frac{\varepsilon_{\mathrm{r},1}d_1+\varepsilon_{\mathrm{r},2}d_2}{d_1+d_2}$ and $\varepsilon_{\mathrm{eff},z} = \frac{\varepsilon_{\mathrm{r},1}\varepsilon_{\mathrm{r},2}(d_1+d_2)}{\varepsilon_{\mathrm{r},1}d_2+\varepsilon_{\mathrm{r},2}d_1}$. As a result, equation (S64) indicates that the photonic crystal can be equivalent to a homogeneous achromatic uniaxial medium with an effective relative permittivity $\bar{\bar{\varepsilon}}_{\mathrm{r}} = \mathrm{diag}\left[\varepsilon_{\mathrm{eff},\perp}, \varepsilon_{\mathrm{eff},\perp}, \varepsilon_{\mathrm{eff},z}\right]$. This way, the dispersion for achromatic Cherenkov radiation can be obtained by further enforcing $k_z = \omega/v$, as derived by equations (6)-(7) in the main text.

S3.2 Robustness of achromatic interfacial Cherenkov radiation on the electron velocity

In this subsection, we analyze the robustness of achromatic interfacial Cherenkov radiation on the electron velocity. As illustrated in Fig. S3(a), when the electron velocity v slightly deviates from the critical velocity v_{B} (e.g. $v/v_{\mathrm{B}} \in [0.9,1.05]$), the radiation peak angles of achromatic interfacial Cherenkov radiation and Cherenkov radiation in effective uniaxial medium remain almost the same. Upon closer inspection by following section S3.1, one has the dependence of the interfacial Cherenkov radiation peak angle θ_{peak} on the electron velocity v, namely

$$\begin{cases} g(\theta_{\mathrm{peak}}, v, \omega) = \cos\left(\frac{\omega}{v}d\right) - \left[\cos\left(\frac{\omega}{c}\sqrt{\varepsilon_{\mathrm{r},1} - \sin^2\theta_{\mathrm{peak}}}d_1\right)\cos\left(\frac{\omega}{c}\sqrt{\varepsilon_{\mathrm{r},2} - \sin^2\theta_{\mathrm{peak}}}d_2\right) - f(\theta_{\mathrm{peak}})\sin\left(\frac{\omega}{c}\sqrt{\varepsilon_{\mathrm{r},1} - \sin^2\theta_{\mathrm{peak}}}d_1\right)\sin\left(\frac{\omega}{c}\sqrt{\varepsilon_{\mathrm{r},2} - \sin^2\theta_{\mathrm{peak}}}d_2\right)\right] \\ f(\theta_{\mathrm{peak}}) = \frac{1}{2}\left[\frac{\varepsilon_{\mathrm{r},2}\sqrt{\varepsilon_{\mathrm{r},1}-\sin^2\theta_{\mathrm{peak}}}}{\varepsilon_{\mathrm{r},1}\sqrt{\varepsilon_{\mathrm{r},2}-\sin^2\theta_{\mathrm{peak}}}} + \frac{\varepsilon_{\mathrm{r},1}\sqrt{\varepsilon_{\mathrm{r},2}-\sin^2\theta_{\mathrm{peak}}}}{\varepsilon_{\mathrm{r},2}\sqrt{\varepsilon_{\mathrm{r},1}-\sin^2\theta_{\mathrm{peak}}}}\right] \end{cases} \tag{S65}$$

where $f(\theta_{\mathrm{peak}})$ is an auxiliary function used to characterize the deviation from the impedance matching

condition which enables the emergence of perfect achromatic interfacial Cherenkov radiation. This way, as further shown in Fig. S3(b), the robustness of achromatic interfacial Cherenkov radiation on particle velocity is fundamentally tied to the robustness of the impedance-matching condition, namely $f(\theta_{\mathrm{peak}}) = 1$.

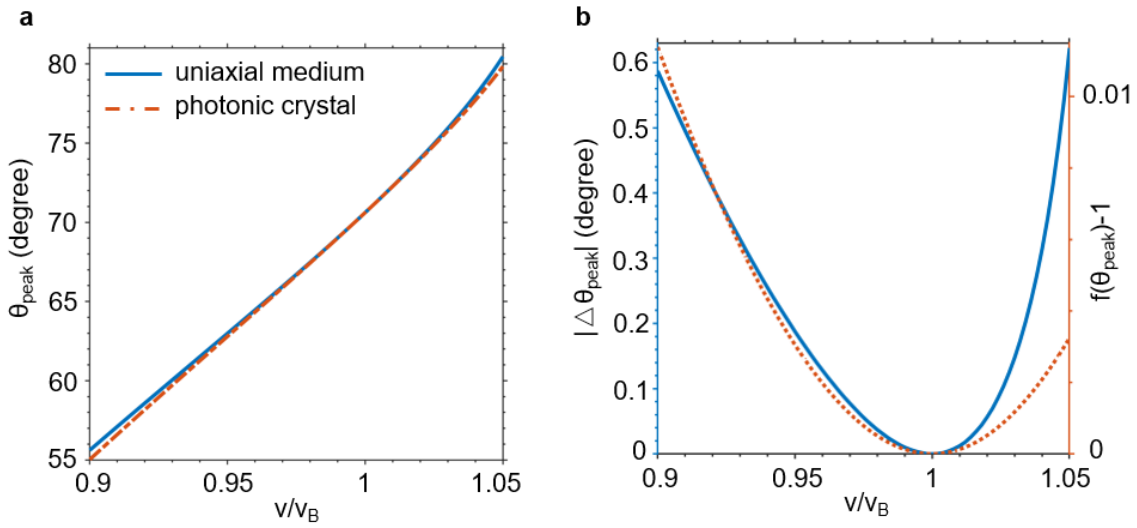

FIG. S3. Robustness of achromatic interfacial Cherenkov radiation on the electron velocity. For illustration, the structural setup of the photonic crystal and its homogenized uniaxial counterpart are the same as that in Fig. 3, and we set the working wavelength $\lambda = 700$ nm in this figure. (a) Dependence of the radiation peak angle on the electron velocity. Here v is chosen to slightly deviates from the critical velocity v_{B}. (b) Dependence of $|\triangle\theta_{\mathrm{peak}}|$ and $f(\theta_{\mathrm{peak}}) - 1$ on the electron velocity.

S3.3 Robustness of achromatic interfacial Cherenkov radiation on the material dispersion

In this subsection, we show the robustness of achromatic interfacial Cherenkov radiation on the material dispersion. To be specific, we investigate how the interfacial Cherenkov radiation manifests in presence of material dispersion in its constituent materials within the working wavelength range $[380, 1100]$ nm in Fig. S4. Moreover, in the infrared-microwave spectrum, while there are abundant choices of dielectrics with negligible dispersion, it is thus safe to use achromatic constituent materials for achieving broadband achromatic interfacial Cherenkov radiation from photonic crystals, as shown in the figures of the main text.

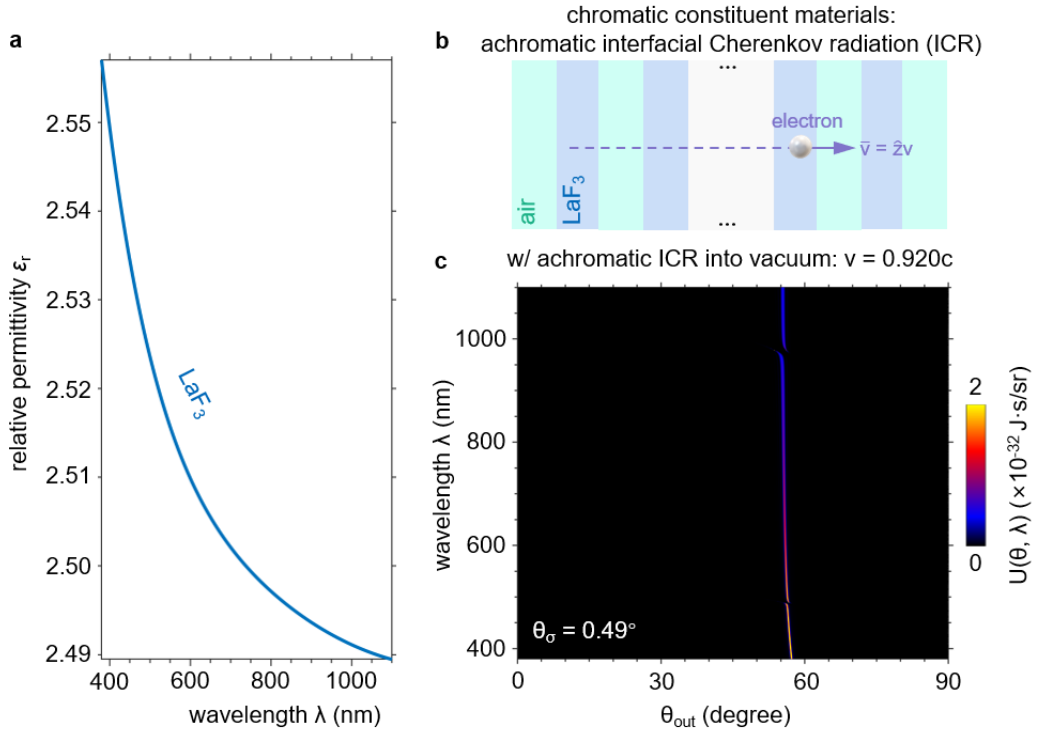

FIG. S4. Achromatic interfacial Cherenkov radiation from finite-thickness photonic crystals with chromatic constituent materials. For conceptual illustration, here the constituent materials of the photonic crystal are air and LaF_3 [109] respectively. The photonic crystal consists of 400 unit cells with $d_1 = 150$ nm (air), $d_2 = 300$ nm (LaF_3). Both the substrate and superstrate are air. (a) Dispersion curve of the photonic crystal constituent materials. (b) Structural schematic. (c) Angular spectral energy density $U(\theta_{\text{out}}, \lambda)$ of forward light emission. In (c), achromatic interfacial Cherenkov radiation (as defined by $\theta_\sigma < 0.5°$) emerges with $\theta_\sigma = 0.49° < 0.5°$.

S3.4 Relationship between the photonic-crystal band diagram and the resulting interfacial Cherenkov radiation

In this subsection, we show relationship between the photonic-crystal band diagram and the resulting interfacial Cherenkov radiation. As shown in Figs. S5(a) and S5(b), when the unit-cell thickness is beyond the subwavelength regime (e.g. comparable to the working wavelength of light), a regular band diagram typically characterized by the existence of band gaps at non-Brewster angles can emerge if $k_z \neq \omega/v_B$ (or

if $v \neq v_B$), and the resulting interfacial Cherenkov radiation is highly sensitive to the working wavelength. In contrast, as shown in Figs. S5(c) and S5(d), an untrivial band diagram free of band gaps at the Brewster angle can emerge if $k_z = \omega/v_B$ (or if $v = v_B$), and the resulting interfacial Cherenkov radiation is essentially achromatic, even if the unit-cell thickness is comparable to the working wavelength of light.

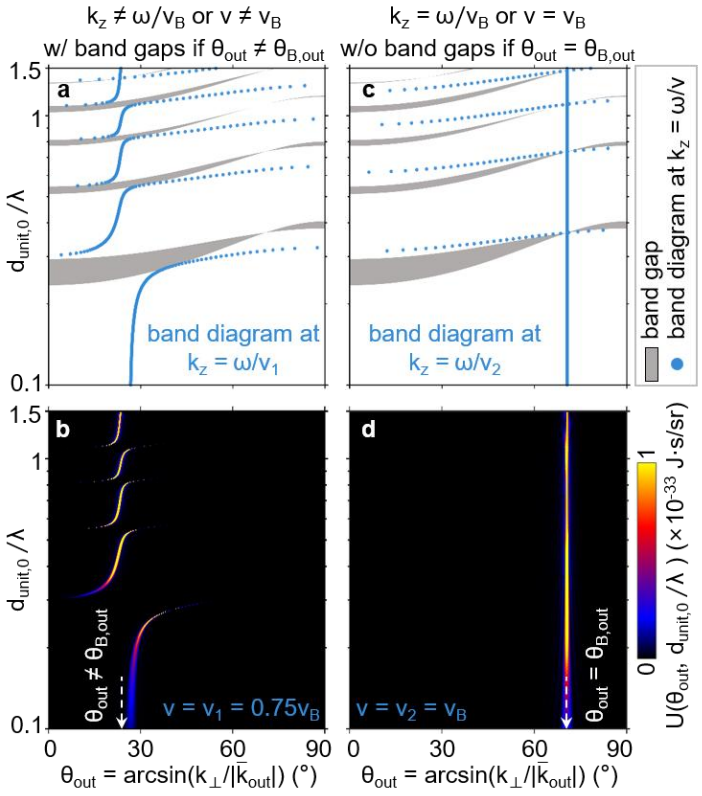

FIG. S5. Relationship between the photonic-crystal band diagram and the resulting interfacial Cherenkov radiation. The structural setup is identical to that in Fig. 2 of the main text. (a) and (c) Photonic-crystal band diagram. The band-gap regions are shaded in gray, and the blue dots denote the band diagram for the excited Bloch modes by the free electron in photonic crystals, satisfying the phase-matching condition $k_z = \omega/v$. (b) and (d) Angular spectral energy density of interfacial Cherenkov radiation for different particle velocities. By tuning the particle velocity so that the excited modes are emitted at the Brewster angle, the band diagram becomes free of band gaps, even when the unit-cell thickness is comparable to the wavelength of light. Correspondingly, the resulting interfacial Cherenkov radiation is fundamentally achromatic.

S3.5 Influence of unit-cell number on the directionality of interfacial Cherenkov radiation

In this subsection, we investigate the influence of unit-cell number N on the directionality of interfacial Cherenkov radiation. Generally, the performance of interfacial Cherenkov radiation (e.g. the directionality) improves as the unit-cell number N increases. For example, in Figs. S6(a) and S6(b), the angular spread θ_σ of the radiation peak angle $\theta_{\mathrm{peak}}(\lambda)$ becomes smaller if N increases. Specifically, as shown in Fig. S6(c), for the photonic crystals used in Figs. 2 and S4, the threshold for the unit-cell number to achieve the condition of $\theta_\sigma < 0.5°$ is 40, namely $N_\mathrm{c} = 40$.

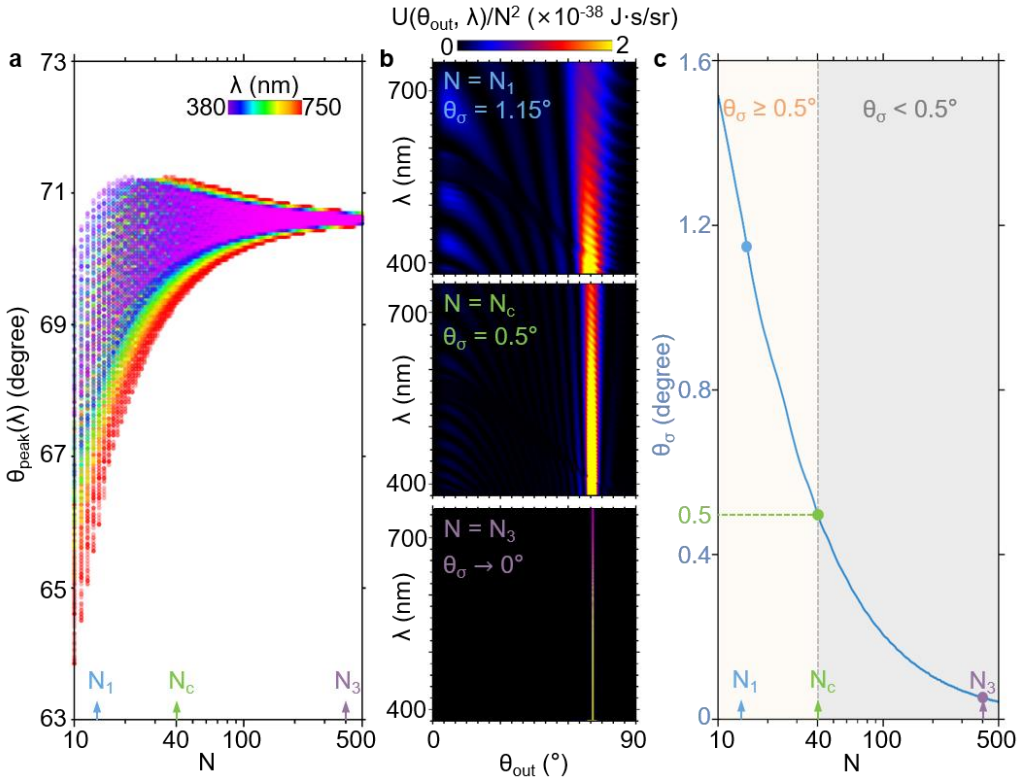

FIG. S6. Influence of unit-cell number on the interfacial Cherenkov radiation. The structural setup is identical to that in Fig. 2 of the main text. (a) Dependence of the radiation peak angles $\theta_{\mathrm{peak}}(\lambda)$ on the unit-cell number N for various working wavelengths within the visible spectrum. (b) Normalized angular spectral energy density $U(\theta_{\mathrm{out}}, \lambda)/N^2$ for various unit-cell number N. (c) Dependence of angular spread θ_σ on the unit-cell number N. The critical value of unit-cell number N_c satisfying the condition of $\theta_\sigma(N_\mathrm{c}) = 0.5°$ is 40, namely $N_\mathrm{c} = 40$.

Reference

108. W.C. Chew, *Waves and fields in inhomogenous media*. (John Wiley & Sons, 1999).
109. M.N. Polyanskiy, Refractiveindex.info database of optical constants. *Sci Data* **11**, 94 (2024).